Gypsum Cements in Cenozoic Sediments in the Murray Basin, South Australia: their Age and Origin

Brett Peter Thomas B.Sc.

Australian National Grid Reference

Renmark sheet SI 54/10
1:250 000

TABLE OF CONTENTS

page

LIST OF FIGURES

LIST OF PLATES

ACKNOWLEDGMENTS

ABSTRACT

A maximum Pleistocene (~0.6 Ma) age has been assigned to surface and sub-surface gypsum cements occurring in the Norwest Bend Formation and Upper Morgan Limestone, in the western Murray Basin. The gypsum cements post date the draining of Lake Bungunnia and the formation of the Murray River Gorge. The chemical and morphological diversity exhibited by the gypsum forms indicates a variety of genetic processes. Three main gypsum facies can be distinguished by their structural fabrics, which are indicative of the environmental conditions in which they formed. (1) Bedded gypsum crusts (selenite) and gypsum nodules have fibrous to lenticular crystals and occur as discrete horizons along sections of the Murray River cliffs. (2) Massive crystalline gypsum contain piokilitic inclusions of clastic material, indicating they formed below the surface where long periods of stable brine conditions allowed for large crystal growth. (3) Aeolian seed gypsum dunes derived from the deflation of gypsum from modern playa lakes. (4) Gyp sum amust

Sulphur and Strontium isotopes, fluid inclusion studies, and geochemical analysis (XRD) and (XRF), were used to interpret the brine conditions under which the different gypsum facies formed. Fluid inclusion analysis was used to determine the palaeosalinity of the brines from which the gypsum precipitated. The melting temperatures of ice in fluid inclusions indicate that brine salinities and compositions were similar to brines derived from evaporated sea water. They also indicate that gypsum crusts formed from less saline water than selenite and gypsum nodules. The $\delta^{34}S$ ratios of gypsum crusts are also close to seawater values (+17.9‰ to +20.2‰ CDT), indicating marine sulphate is the dominant source of sulphur. Strontium isotope data negate the possibility of derivation of the lacustrine "seawater like" brine chemistry, from either marine transgressions or weathering of connate salts from marine strata alone.

Sulphur and Sr isotope ratios of the gypsum crusts indicate that gypsum was predominantly derived from the dissolution of the aeolian gypsum dunes by meteoric water influenced by sea spray. The demise of Lake Bungunnia indicated the onset of aridity in Southern Australia. The draining of the megalake may be responsible for the gypsum cements and the aeolian gypsum dunes from which they were derived.

1. INTRODUCTION

1.1. Aims and Objectives

The aims of this project are to determine the age and origin of various gypsum occurrences within the Cenozoic sediments of the Western Murray Basin. Interpretations of the age relationships, depositional environment and chemistry of the brine waters that precipitated each of the gypsum types are made. These aims are achieved by using fluid inclusion studies, sulphur (S) and strontium (Sr) isotope analysis, X-ray diffraction (XRD) and X-ray fluorescence spectrometry (XRF) of the gypsum samples and associated sedimentary lithologies. Information about palaeo-groundwater salinities and chemistries can be gained from gypsum chemistry. Environmental implications for groundwater management within the Murray Group Aquifers may be ascertained.

1.2. Previous Studies

The Murray Basin has been the focus of many palaeontological studies (e.g. Howchin, 1929 and Crespin, 1944). Major lithostratigraphic, and biostratigraphic studies were undertaken by Ludbrook in a series of reports (Ludbrook, 1958, 1961, 1963). Her main contribution to the literature "Stratigraphy of the Murray Basin in South Australia" in 1961 identified and described 17 different Tertiary rock units on the basis of detailed biostratigraphic analysis from outcrop and borehole samples. Other stratigraphic investigations include Giles, (1972); Harris, (1966); Harris, (1985a); Harris, (1985b); Lindsay and Bonnett, (1973); Lindsay and Williams, (1977); McGowran, (1979); Twidale et al., (1978); Lindsay and Barnett, (1989); Lukasik and James (1998) and Qianyu and McGowran, (1999). Geological investigations were culminated in Sprigg, (1952); O'Driscoll, (1960); Mucumber (1969, 1978); Lawrence, (1966, 1973); Abele, (1976, 1988); Thornton, (1974, 1976); Tickell and Humphrys, (1979), Brown, (1985) and Brown and Stephenson, (1986, 1991). Groundwater investigations were compiled by O'Driscoll, (1960); Lawrence, (1973) and Brown and Stephenson (1986). Studies relating to physiography and morphology have been undertaken by Hills, (1939); Blackburn, (1962); Gill, (1973); Firman, (1973) and Kotsonis, (1995). Gypsum occurrences within the Murray Basin have been described by Lockhart, (1921) and Jack, (1921). Sulphur isotopes and geochemistry of recent gypsum occurrences in saline playa deposits, within South and Western Australia have described by Chivas et al., (1990).

2. GEOLOGICAL FRAMEWORK

2.1. The Murray Basin

The Murray Basin is a shallow, Tertiary, intracratonic basin covering an area of 300,000km^2 (Ludbrook 1960, 1961, Brown and Stephenson 1991). Its surface elevation is generally less than 100 m above sea level. The most extensive outcrops are exposed along cliffs eroded by the Murray River, which runs through the basin. In South Australia, the Murray Basin sediments transgress on to folded Neoproterozoic sediments of the Adelaide Geosyncline, Cambrian metasediments of the Kanmantoo Group, and Cambro-Ordovician granites (Rogers et al. 1995). The eastern margin of the basin is marked by the Lachlan Fold Belt (Tasmanides) and the Otway Basin to the south (Ludbrook 1961) (figure 2.1). To the southwest, the basin is partly separated from the thicker succession of the Gambier Embayment by the Padthaway Ridge (Thornton 1974).

Basement consists of Proterozoic metamorphics of the Kanmantoo Group in the west and north, and Early Paleozoic metasediments of the Lachlan Fold Belt in the east. A number of older infrabasins underlie the Murray Basin in the west-central and northern portions. These basins include the late Paleozoic Troubridge, Nadda and Darling Basins, and the Early Cretaceous Monash Formation sediments of the Berri Basin (Rogers et al. 1995).

The Tertiary succession has a maximum thickness of 600 m in the main depocentre beneath the west-central areas (Renmark), 300-400m beneath the west-central Riverine Plain, and generally less than 200m beneath the northern, eastern and southern areas (Brown 1988) (figure 2.1). The basin comprises undeformed freshwater, marine, coastal and continental sediments of Paleocene to Quaternary age (Ludbrook 1960, 1961, Thornton 1974, Rogers et al. 1995, Lukasik and James 1998). Cenozoic carbonate and terrigenous clastic sedimentary rocks constitute regional and locally important groundwater aquifers (e.g. O'Driscoll, 1960, Stephenson 1986).
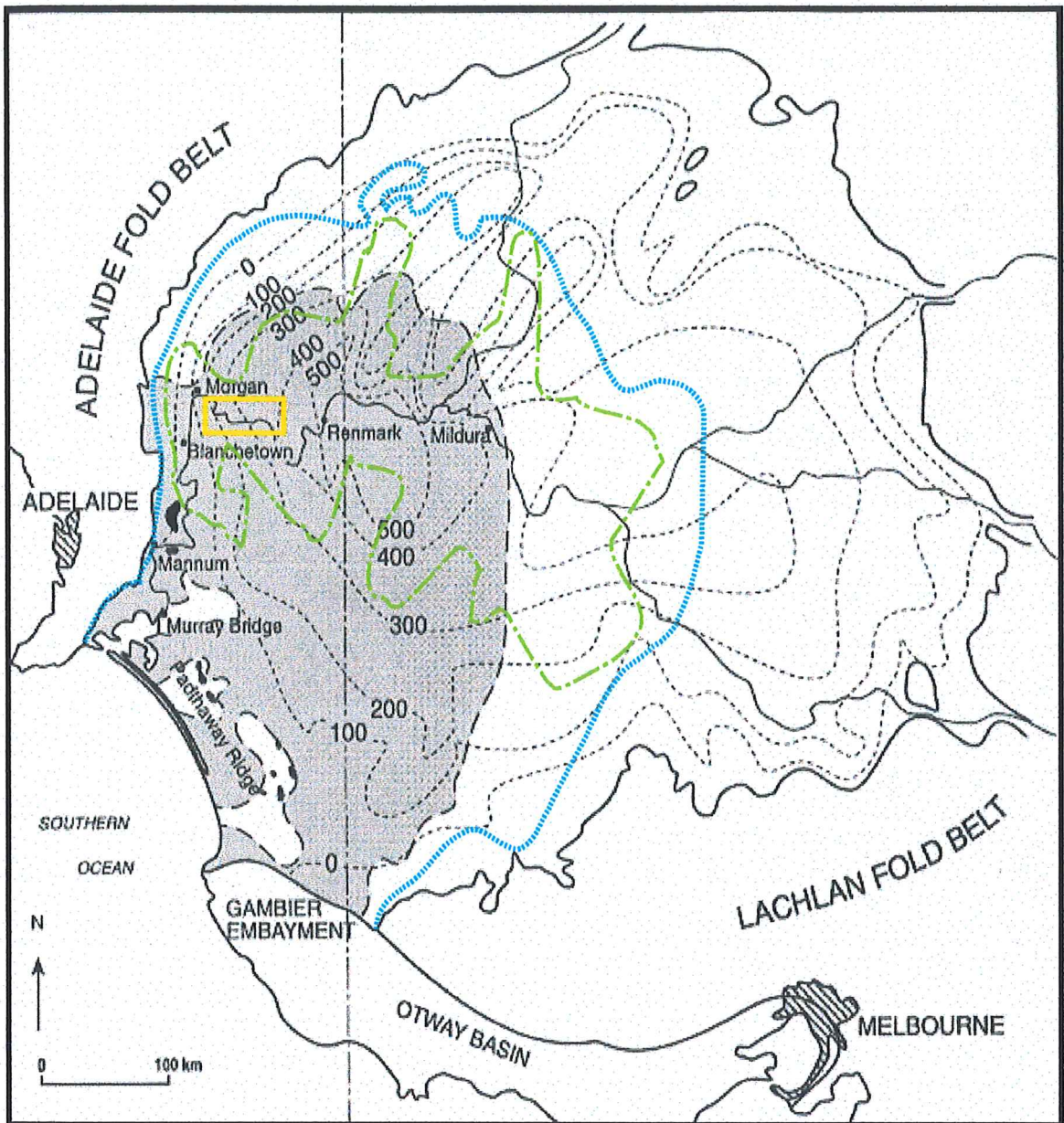
Figure 1. 2 :

Murray Basin (after Brown, 1981) showing the distribution of the Murray Group Limestones and granitoids. Structure contours show the base of the Tertiary in meters.

- ─ ─ 200 ─ ─ ─ Structure contours of basal Tertiary
- Murray Group Limestones
- ·········· Maximum extent of marine influx
- ─·─·─ Maximum extent of Lake Bungunnia
- Granitoids
- Study area (see fig. 3a.)

3
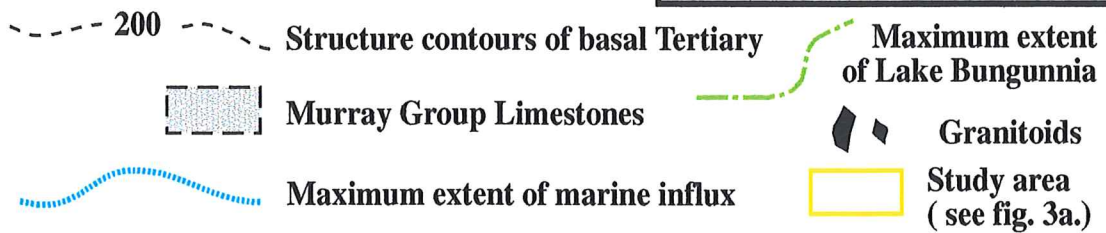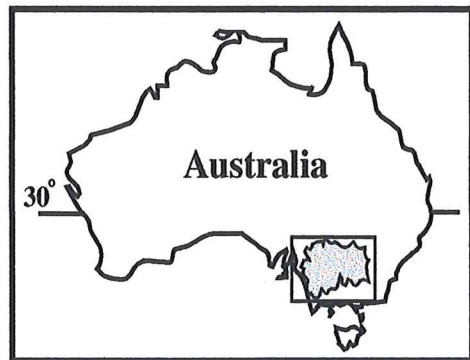
2.2. Murray Basin Stratigraphy

The Tertiary sedimentary sequences of the Murray Basin are complex due to the migration of sea levels and river courses. Marine transgressions are restricted to the western part of the basin (Lawrence 1973). The major lithologic units of the Murray Basin are represented in figure 2.2. These include: neritic limestones of the Ettrick Marl; shallow water near-shore clays and marls of the Geera Clay, Winnambool Formation and Bookpurong Formation; fluvial sands of the Olney Formation, Warina Sand and Calivil Sands; and the non-marine clays and silts of the Wunghnu Group (Ludbrook 1960, 1961, Lawrence 1966, 1973, Thornton 1974, Brown 1988, Brown and Stephenson 1991, Macphail 1993, Rogers et al. 1995, Lukasik and James 1998).

The Tertiary sediments are covered by complex Quaternary deposits of aeolian sands and clays (Lower Sand, Woorinen Formation), lacustrine deposits (Blanchetown Clay and Bungunnia Limestone), fluvial sediments (Coonambidgal Formation), piedmount fanglomerates (Tawonga Gravel) and evaporites (Yamba Formation) with lunettes and source-bordering dunes (Brown 1988).

The Tertiary succession can be divided into four depositional sequences defined by their planktonic foramaniferal biostratigraphy, separated by non-depositional or erosive events (McGowran 1979, Brown 1988, Brown and Stephenson 1991, Rogers et al. 1995).
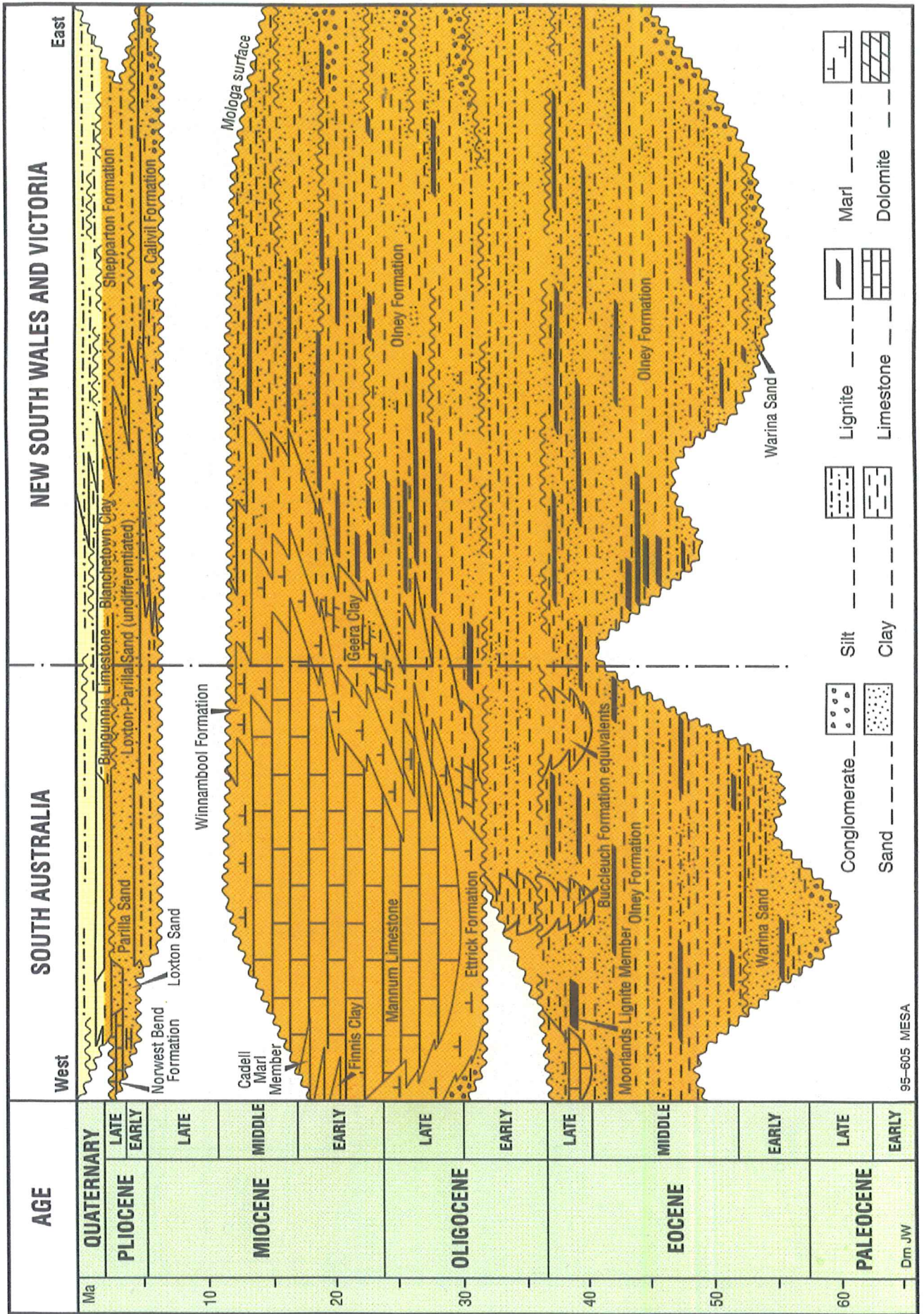
Figure 2.2. Murray Basin stratigraphy (from Brown and Stephenson 1991).

Sequence 1: (Late Paleocene to Oligocene).

Renmark Group:

These sediments consist of the **Warina Sand**, a 200 m thick fluvial unit of weakly consolidated, medium to coarse quartz sands with minor intercalated calcareous fine sand, silt and clay sediments. Marine influences increase towards the top. The Warina Sand is overlain by the **Olney Formation**, an unconsolidated, thinly bedded calcareous silt, sand and clay which contains carbonised and pyritic plant remains, lignite coal and peat. The **Buccleuch Beds** contain shallow marine glauconitic calcareous clays, thin bryozoan limestones and minor calcareous sands (Rogers et al. 1995).

Sequence 2: (Oligocene to Middle Miocene).

Murray Group:

The **Compton Conglomerate** has a patchy distribution and is lithologically variable. It comprises residual quartz pebbles with ferruginised matrix, shallow marine glauconitic clays and calcareous sandstones. The **Ettrick Formation** forms the basal unit of Murray Group where the Compton Conglomerate is absent. The 20-30 m thick unit consists mainly of glauconitic calcareous clay (marl) (Ludbrook 1961). The **Mannum Formation** is a mid-shelf facies, bryozoan-rich limestone comprising large fragments within a matrix of fine to medium-grained skeletal debris with varying proportions of calcareous clay, micrite and quartz sand. These are calcarenitic in the west, but become increasingly fine grained toward the southeast (Rogers et al. 1995). To the north, the Mannum limestones grade into the **Finniss Clay**, a narrow zone of glauconitic calcareous, non-fossiliferous clays. The 30 m thick **Morgan Limestone** rests non-conformably on the Finniss Clay (Ludbrook 1961). This Member can been differentiated into Upper and Lower sections, being separated by the **Cadell Marl Lense** (equivalent to the **Overland Corner Clay** near Overland Corner). The Cadell Marl represents a deep marine environment, between 2 shelf limestones containing abundant fossils, including bones from marine mammals (Thomas 1999). The Lower and Upper Morgan Limestones are analogous to the Glenforsian Formation and Bryants Creek Formation respectively, from the revised Stratigraphy of the Murray Supergroup (Lukasik and James 1998). The nomenclature of Lukasik and James (1998) has not been adopted for this report.

The **Pata Limestone**, a gray to white, partially recrystallised, bryozoal limestone forms the top 15 m of the Murray Group (Ludbrook, 1961). Toward the west, this unit grades into the **Geera Clay**, a black, carbonaceous, silty quartz rich mud and clay with minor dolomite and sand intercalations (Brown and Stephenson 1991).

Sequence 3: Late Miocene to Pliocene

The shallow-marine **Bookpunga Beds** contain green, gray and yellow micaceous and glauconitic sands and marls with abundant mollusca (Ludbrook 1961). They are bound to the north and east by the marginal marine **Loxton-Parilla Sands**. These undifferentiated sands are fossiliferous, cross-bedded, micaceous, coarse to silty sands, which are flanked to the north and east by the fluvial and fluvio-lacustrine Calivil Formation. The **Calivil Formation** forms an extensive sheet underlying the east and north of the Murray Basin. It fills entrenchments within older sediments and the basement rocks of adjacent valleys. The **Norwest Bend Formation** forms several generations of cross cutting and disconformable estuarine and fluvial deposits that are exposed in the River Murray Gorge. It comprises calcareous sandstones with thick estuarine oyster beds that were deposited during a minor rise in sea level in the late Pliocene (Ludbrook 1961).

Sequence 4: (Quaternary)

In the north and east of the Basin, intermittent fluvio-lacustrine sedimentation resulted in development of the modern Riverine Plain. Further west, the Tertiary is partly overlain by the thin Pleistocene fluvio-lacustrine **Blanchetown Clay** and the minor dolomitic limestone deposits of Lake Bungunnia (Stephenson 1986). Lake Bungunnia covered a portion of the central-western Murray Basin, and was formed by the tectonic damming of the proto-Murray River by the uplifted Pinnaroo Block (~2.5 Ma) (figure 2.1). Erosion of the dam, or drying by the onset of aridity, or a combination of both, led to the demise of the megalake, and the formation of modern landforms in the Murray Basin. Lake Bungunnia deposits are covered by aeolian sediments of the **Woorinen Formation** and **Molineaux-Lowan Sands**. Fluvial sedimentation continues within the confined flood plains of modern rivers.

3. LOCAL GEOLOGY

3.1. Gypsum within the Western Murray Basin

Gypsum crusts are found in arid and semi arid regions where mean monthly evaporation exceeds mean monthly precipitation. Gypsum rarely forms in regions where annual rainfall exceeds 250mm (Watson 1985). When moisture availability exceeds evaporation, meteoric water will dissolve surface and near-surface gypsum accumulations and transport them into the soil, and eventually to the groundwater interface (Watson 1985). Subsurface crusts may result as the gypsum precipitates at the water table where it approaches the land surface and undergoes evaporation (Watson 1983b). These crusts, comprising loose, powdery or cemented, crystalline accumulations of calcium sulphate dihydrate ($CaSO_4.2H_2O$) are usually found at the surface or within the uppermost 10 m of the regolith. Thicknesses vary from a few millimeters to several meters. Gypsum content ranges from about 15% to nearly 100% (Watson 1983a).

Gypsum is susceptible to dissolution and reprecipitation, resulting in marked chemical and textural changes. Care should therefore be taken when using it as a palaeoenvironmental indicator. However, when primary gypsum is identified, it can provide valuable indicators of past hydrological, climactic and pedogenic events in many arid environments (Watson 1985). Gypsum occurrences within the Murray Basin have been described by Lockhart (1921), who identified 5 different types such as "rock gypsum", granular scattered gypsum, "seed" or the finer "flour" gypsum, and crystalline gypsum layers. These gypsum varieties were found to exist within the study area (figure 3.1a) and are described below.
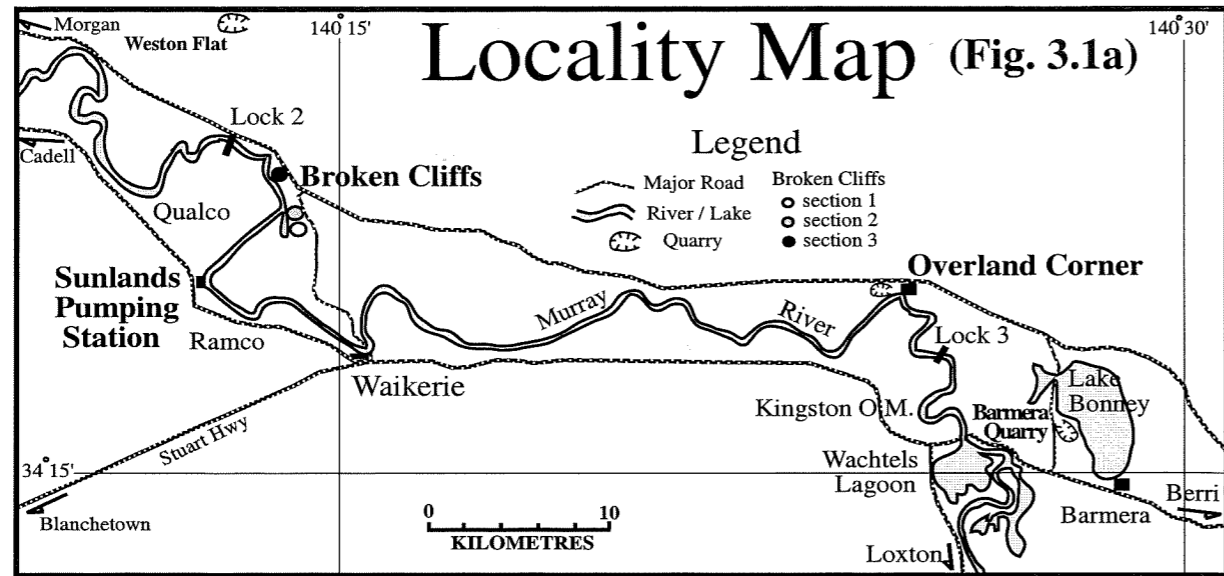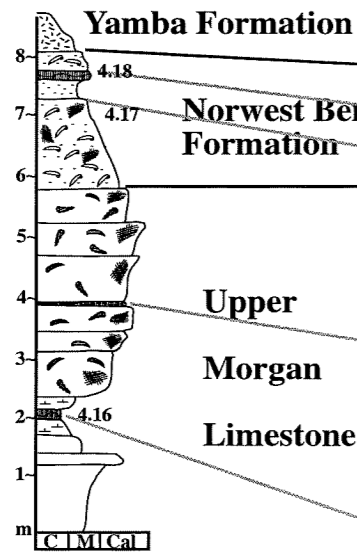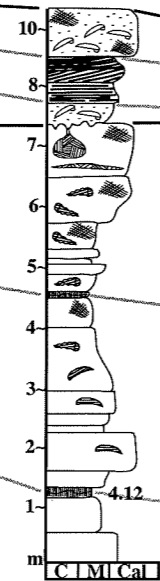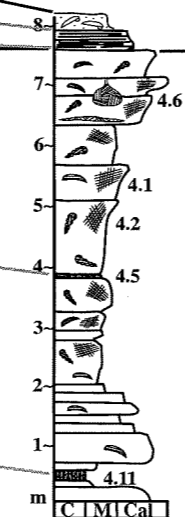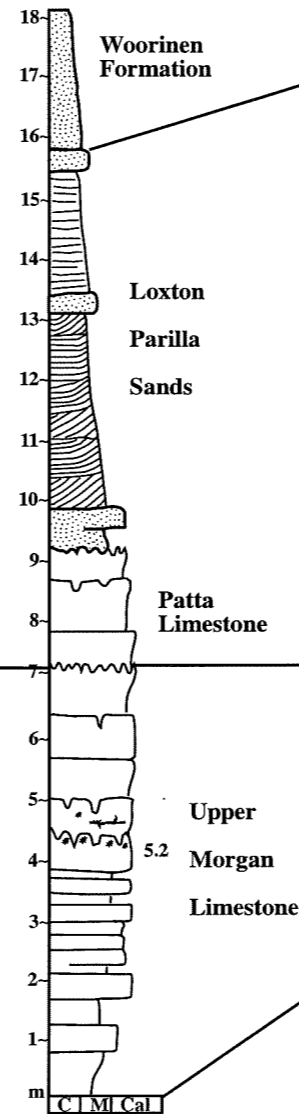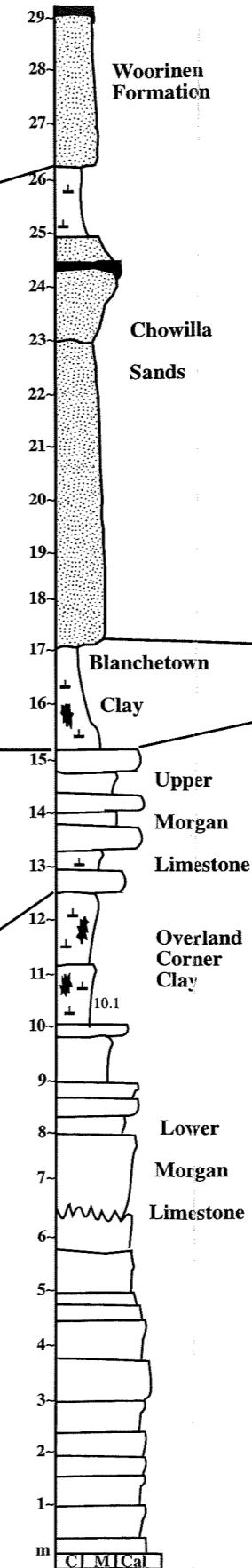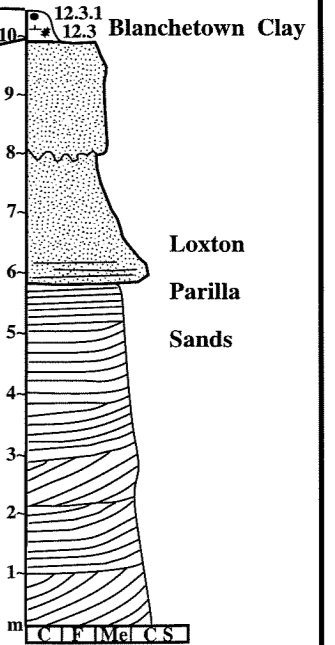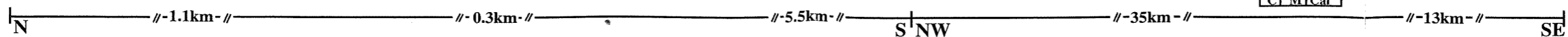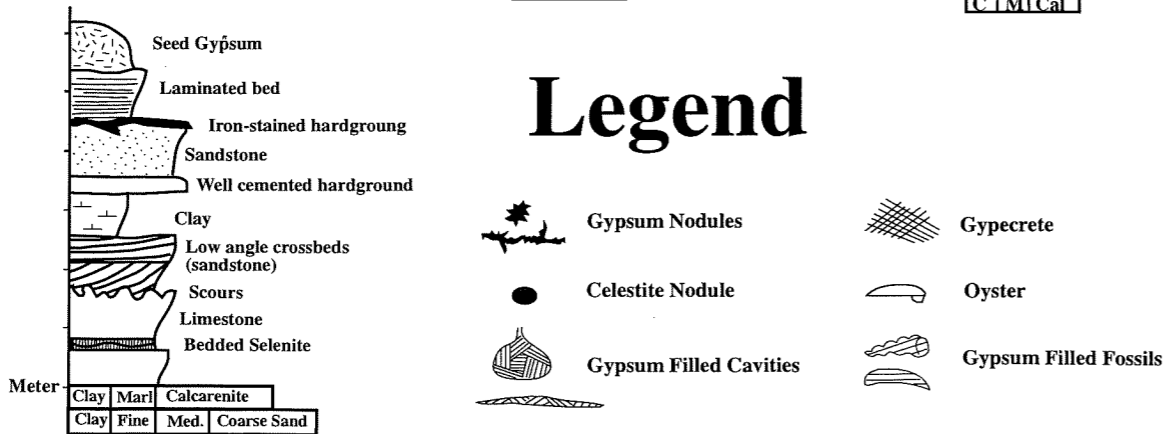
Figure 3.1 Local Geology

Generalised lithostratigraphic correlation of the Murray Basin sediments exposed at each locality.

(B. P. Thomas 1999)

3.1.1. Gypsum nodules from the Miocene Overland Corner Clay (Cadell Clay).

The Overland Corner Clay contains large, oval, gypsum nodules, ranging from 10 to 35 cm long (Plate 3.F). They consist of vertical orientated lenticular, and prismatic radiating gypsum crystals. The radiating nature of the prismatic gypsum crystals is suggestive of a displacive origin, forming within the clay (Ali 1983).

3.1.2. Gypsum from the Upper Morgan Limestone

Gypsum within the Upper Morgan Limestone occurs in 5 main forms: gypcrete, fossil replacement (small cavity fills), massive selenite cavity fills, nodular gypsum and bedded selenite. The cliff section at **Broken Cliffs** (Section 1) exposes 9.5 m of Upper Morgan Limestone, (the Bryants Creek of Lukasik and James 1998). Set back about 20 m to 100 m from the cliff top is a 0.5-1 m thick section of ferricreted fine to coarse sandstone, representing the Norwest Bend Formation. Although gypsum is not visible in the Norwest Bend Formation at this locality, it is extensive within the Upper Morgan Limestone, assuming a number of morphologies and positions within the section (figure 3.1).

The hard ground immediately below the Norwest Bend Formation is also gypsum free. However, immediately below this layer, gypsum occurs as **massive, mesocrystaline selenite** filling cavities, **bedded selenite** and **gypcrete**. Selenite fills vertical and horizontal cracks (0.5-3 cm thick), spherical karsts (up to 0.8 m across), and forms near-horizontal lenses up to 3 m long and 20 cm thick with randomly orientated crystals up to 3 cm long (Plate 1.E, Plate 2.C) (sample 4.5). These forms of massive gypsum only occur in the top 2.5 m of the Upper Morgan Limestone cliff section. Gypcrete and small gypsum filled cavities are extensive, occurring throughout the upper 5 m of the cliff (Plate 1.C) (Sample 4.1). A 1-2 cm thick, horizontal, **bedded selenite** layer (samples 4.6) occurs below the gypcrete zone (Plate 1.F). The selenite bed lenses out 15 m to the east, but becomes increasingly thicker (up to 10-15 cm) westward along the cliff face, persisting the entire length of the cliff (1.1 km westward to Section 3).

The cliff face has been extensively quarried by amateur fossil collectors for **gypsum replaced fossils** (figure 3.2) (sample 4.2), which are common above this thin, gypsum layer. The most common pseudomorphs are of conical *Turritella murrayana* shells, other gastropods, brachiopods, bivalves and solitary corals (Ludbrook 1961) (figure 3.3, Plate 1.D). Rare, but very impressive Nautilus shell and crab carapace casts are also known to occur. These fossil casts are the result of the gypsum filling the cavities left after the aragonite and calcite shells had been dissolved by meteoric water. They are found within gypcrete and between gypcreted zones. The gypsum cleavage is often parallel in both settings where they are adjacent, suggesting their formation was synchronous. Much of the intergranular gypsum (gypcrete) has therefore been leached preferentially from the cliff section, leaving the more massive, mesocrystaline, cavity filling gypsum. The remaining gypcrete zones occur as rough columns, 0.3 to 2 m across, extending up to 3 m vertically. Dissolution of gypsum casts by rainwater occurs on the top of exposed surfaces (Plate 1.I). The surface runoff has re-precipitated the gypsum as a 1-2 mm thick crust on the surface of recently excavated cliff faces (Plate 1.G).

At the base of the cliff (3.3 m below the thin selenite layer), a thicker **selenite** (samples 4.11, 4.12, 4.16) layer extends the entire length of the cliff (Plate 1.H). It is 15 cm thick and occurs within a recessive, dark gray / green clay, 40 to 50 cm thick (Plate 2.F, 2.G). The lower selenite bed contains vertically orientated gypsum crystals up to 10 cm long and 0.5 cm wide (Plate 2.H). The vertically orientated crystals suggest the gypsum precipitated from a standing body of water (Attia et al. 1995).
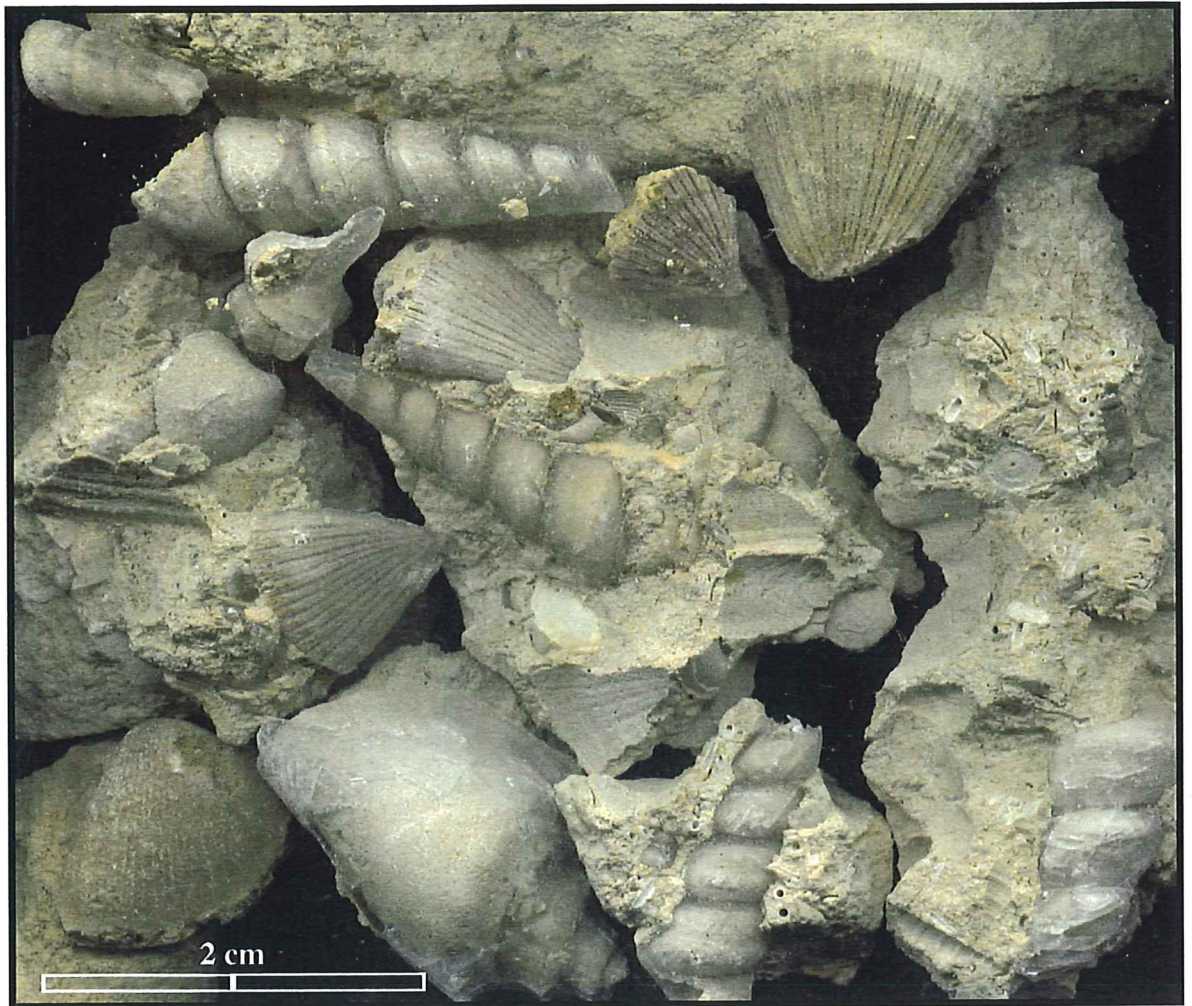
Figure 3.2. Common gypsum pseudomorphs from the Upper Morgan Limestone at Broken Cliffs. Conical Turritella murrayana sp. and other gastropods, brachiopods, bivalves and solitary corals are shown. Rare, spectacular Nautilus shells and crab carapase casts have also been collected from Broken Cliffs.

Along the cliff section at the **Sunlands pumping station** (Plate 3.A), gypsum occurs as nodular aggregates and small, bedding parallel lenses within clay-rich beds of the Upper Morgan Limestone (Plate 3.D). Gypsum layers also occur between channel casts, along the eroded bedding plane and appear to be cut off by these scours (Plate 3.C) (sample 5.2). Small gypsum nodules also occur in the overlying (erosive) marl bed (sample 5.6). Although this suggests the gypsum predates the overlying marl, the gypsum crystals within the nodules and eroded layer, are randomly orientated prismatic crystals, suggesting a displacive origin (Schreiber et al. 1982). The host clay may have a higher sulphur content than the surrounding marl, forming nodular gypsum after burial as the Ca-rich water reacted with sulphate within the clay (Lockhart 1921). Smaller gypsum nodules occur along vertical cracks and spread out along bedding planes. These nodules are often associated with gypsum cemented brecciated host rock (figure 3.3).

Figure 3.3. Crack filling, nodular gypsum and gypcrete (pseudo-breccia) from the Upper Morgan Limestone, Sunlands Pumping Station (sample 5.6).

13

3.1.3. Gypsum from within the Pliocene Norwest Bend Formation

Gypsum within the Norwest Bend Formation only occurs at Broken Cliffs, (Sections 2 and 3). It occurs in 3 forms: flour gypsum (gypseous earth), gypcrete, and bedded selenite (Plate 2.D, 2.E). The Norwest Bend formation at Broken Cliffs ranges from 0.5m thick at Section 1, to 6m thick at Section 3 (figure 3.1). **Flour and Seed gypsum** forms a soft, unconsolidated cover on top of Sections 2 and 3, ranging from 0.2 m to 1 m thick respectively, but is absent from section 1. This gypsum is most likely due to the breakdown of the underlying, more massive form (Lockhart 1921). Gypsum flour deposits in the form of aeolian dunes (Yamba Formation) exist 10km to the northwest, near Weston Flat, where they are presently being worked for agricultural use (sample gyp.mine) (figure 3.4). These deposits may have been contributed to by seed and flour gypsum being blown out of dry saline lakes (Lockhart 1921), in a similar manner to the vast White Sands dunes in central New Mexico (Y. Bone, pers comm. 1999).
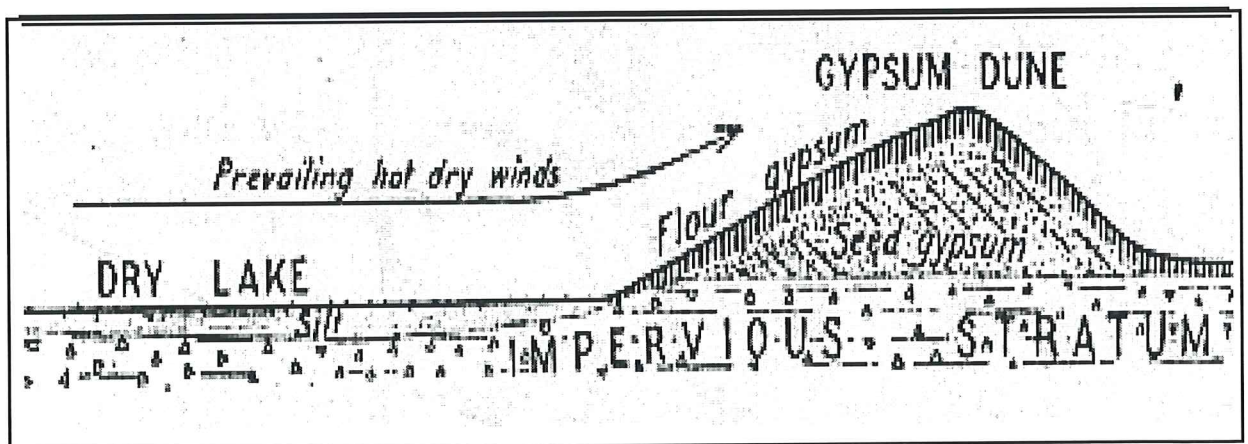
Figure 3.4. Sketch showing the formation of recent "seed" and "flour" gypsum dunes within the Murray Basin. Microcrystalline gypsum forming from the evaporation of saline lakes and playas is blown into dunes fringing the lakes (from Lockhart 1921).

The Norwest Bend Formation at Broken Cliffs is predominately a weathered, poorly sorted, fine to coarse grained sandstone, dominated by oyster shells. This unit ranges from 6 m thick, of Section 3 to 0.3 m thick at Section 1. A coarse to fine, laminated and cross-bedded sand up to 1 m thick forms the base of the Norwest Bend Formation at Section 2. This sand unit is 0.2 m thick at Sections 1 and 3, where it is iron stained and cemented. At Section 2, it is well cemented, often forming overhangs along the cliff top (Plate 2.B). The unit is gypsum-cemented at Sections 2 and 3, forming massive, clear crystals between and within oyster shells (sample 4.17) (Plate 2.E). **Bedded selenite** outcrops for about 35 m along the cliff face, forming a 20 to 25 cm thick, horizontal hardground within the gypsum-cemented oyster beds (sample 4.18). It occurs 2.2 m above the Upper Morgan Limestone (Plate 2.D).

3.1.4. Gypsum within Pliocene Blanchetown Clay

The Blanchetown Clay contains large, oval gypsum nodules, ranging from 20 cm to 35 cm long that appear similar to gypsum nodules within the Overland Corner Clay. They consist of prismatic, radiating gypsum crystals, forming a "rose" around a core of laminated, lenticular crystals (sample 12.3) (plate 3.F). The prismatic nature of the gypsum crystals is suggestive of displacive growth, within the clay. Small celestite ($SrSO_4$) nodules are also present in the clay (sample 12.3.1), and may have replaced some gypsum nodules (figure 3.5).

Figure 3.5. Celestite nodule replacing gypsum nodules within the Blanchetown Clay at the Barmera quarry. (Sample 12.3.1). Nodule diameter is 7 cm.

Plate 1.

Gypsum varieties at Broken Cliffs (section 1).

Plate 1.A: Upper Morgan limestones at Broken Cliffs (section 1). Gypcrete and gypsum (fossil) pseudomorphs are most common within the upper half of the cliff section. Measuring staff to the left of the photo is 2 m long.

Plate 1.B: Quarried section of cliff at Broken Cliffs, section 1. Goran, (in the middle of the photo) is 1.8m tall. The thin selenite bed is visible along the cliff, in the left of the photo (Goran's ankle height). It lenses out to the to the right.

Plate 1.C: Residual gypcreted portion of calcarenite within the Upper Morgan at Broken Cliffs, section 1. The entire gypecrete clump, occurring near the hammer head has a preferred cleavage, parallel to that of the gypsum. Hammer for scale. (Sample 4.1).

Plate 1.D: Gypsum (fossil) pseudomorphs exposed on the cliff face. Note gypsum cleavage is parallel within the different casts (indicated with an arrow). The pen is 16cm long. (Sample 4.2).

Plate 1.E: Cylindrical shaped karst filled with mesocrystaline, randomly orientated gypsum crystals. The karst occurs 1 m below the top of the Upper Morgan Formation. Note the chimney at the top of the karst (marked with an arrow). Measuring staff intervals are 10 cm. (Sample 4.6).

Plate 1.F: Small, selenite gypsum bed within the Upper Morgan at Broken Cliffs, section 1. Note the random orientation of prismatic gypsum crystals. Ruler is 17 cm long. (Sample 4.5)

Plate 1.G: Gypsum surface crust – the edge is marked with an arrow (sample 4.8). The crust is 1 to 2 mm thick. The crust occurs on the recently quarried cliff face at Broken Cliffs, section 1. Lense cap is 5 cm across.

Plate 1.H: Selenite bed within the Upper Morgan at Broken Cliffs, near section 2. This bed is about 10 cm thick. It lenses out completely, 200 m NNE, near section 1.

Plate 1.I: Calcarenite sample from an exposed surface at the top of the cliff at Broken Cliffs, section 1. Note the small (white) remnants of gypsum within the fossil casts.

Plate 1
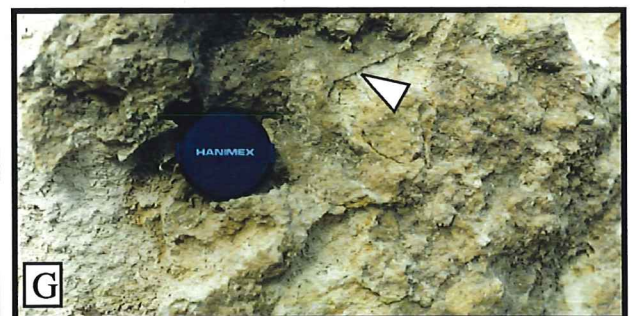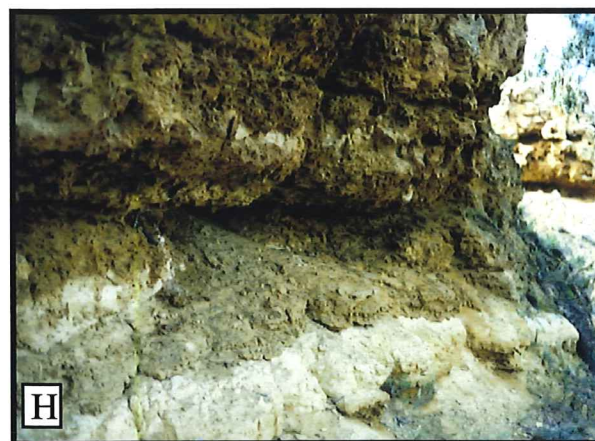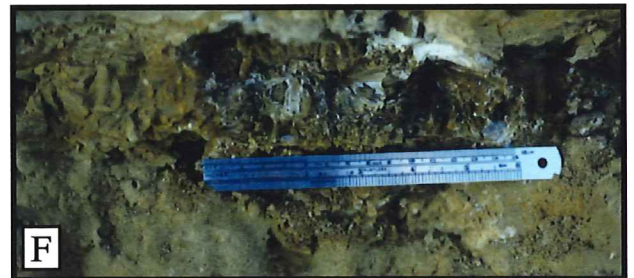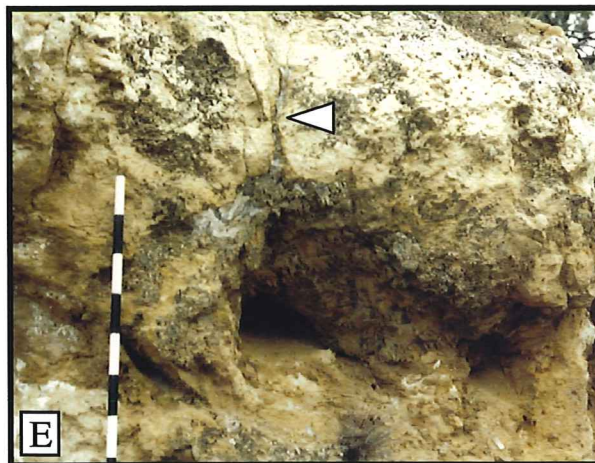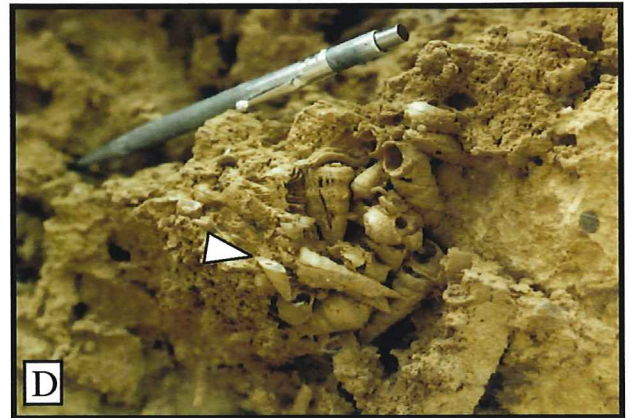
Plate 2.

Broken Cliffs gypsum and geology (sections 2 and 3).

Plate 2.A: Broken Cliffs (section 2) showing the position of the selenite beds within the Upper Morgan Limestone. The Norwest Bend Formation forms the top 2.5 m of cliff. The measuring staff is 2 m long.

Plate 2.B: Norwest Bend sandstone and oyster beds form the top 2.5 meters of the cliff at Broken Cliffs, section 2. The measuring staff is 2 m long, and rests on the top of the Upper Morgan Limestone.

Plate 2.C: Massive, crystalline gypsum within a lense shaped void within the Upper Morgan Limestone at Broken Cliffs, section 2. Hammer for scale.

Plate 2.D: Selenite bed (sample 4.18) within the Norwest Bend Formation, Broken Cliffs, section 3. The measuring staff is 2 m long.

Plate 2.E: Gypsum cemented oyster bed, Norwest Bend Formation, Broken Cliffs, section 3. The pen is 16 cm long. (Sample 4.17).

Plate 2.F: The removal of the selenite bearing clay bed by the Murray River in flood, has produced these impressive overhangs within the Upper Morgan at Broken Cliffs, near section 3. The gap is about 40 to 50 cm wide, and is the cause of cliff failure at Broken Cliffs.

Plate 2.G: Selenite bed within a green clay layer at the base of the cliff at Broken Cliffs, section 3. The lense cap is 5 cm across. (Sample 4.16).

Plate 2.H: Lenticular selenite to the base of the cliff at Broken Cliffs, section 3. Note the near vertical orientation of gypsum crystals and clay layers between growth bands. (Sample 4.16).

Plate 2

oyster beds

sandstone

limestone

seed gypsum

selenite bed

2cm
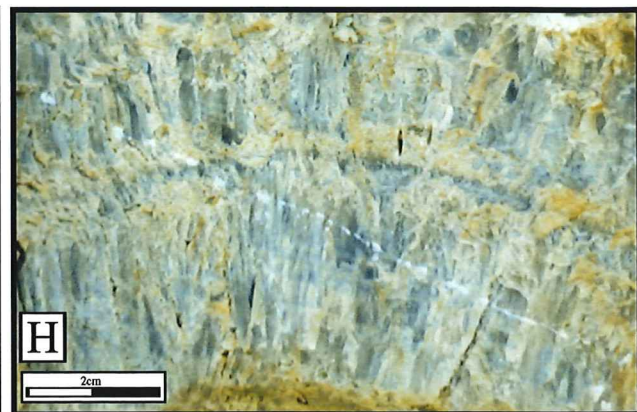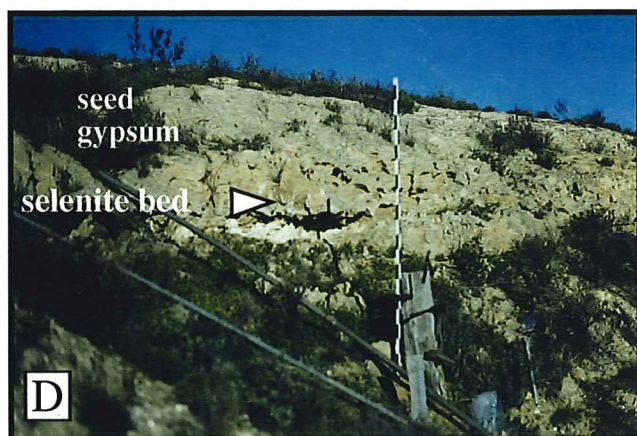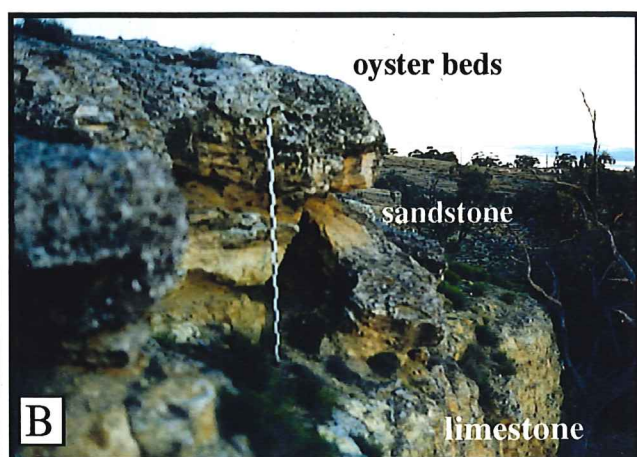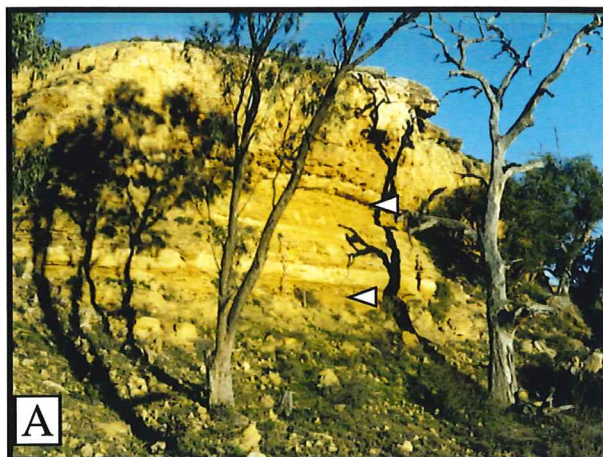
Plate 3.

Geology and gypsum at Sunlands, Overland Corner and the Barmera Quarry.

Plate 3.A: Top section of the cliff at the Sunlands pumping station.

Plate 3.B: Low-angle cross-beds within the Loxton Sands. The Upper Morgan Limestone occurs 2.7 m below the top of the Pata Limestone. The sledge hammer at top left of the photo is 1 m long.

Plate 3.C: Gypsum nodules within a scoured marl, below a calcarenite bed. Hammer for scale.

Plate 3.D: Gypsum nodules within the calcarenite bed, just above the scoured marl. The ruler is 17 cm long.

Plate 3.E: Pleistocene Woorinen Formation, Chowilla Sands and Blanchetown Clay above the Upper Miocene, Upper Morgan Limestone at Overland Corner. Jon is for scale.

Plate 3.F: Gypsum nodule from within the Overland Corner Clay at Overland Corner. Note the growth bands within vertically orientated lenticular gypsum crystals.

Plate 3.G: The Overland Corner Clay (Cadell Marl equivalent) and Lower Morgan Limestone exposed within the Overland Corner Quarry, near the Overland Corner Hotel.

Plate 3.H: Loxton/Parilla Sands exposed in the Barmera quarry. Small cross-beds occur near the bottom left of the photo. The silicified sandstone forms scours within the top of the glauconitic sandstone. The Blanchetown Clay forms a gray-green, cracking clay on top of the silicified sandstone.

Plate 3

A — Woorinen Fm. / Loxton Sands / Pata Limestone

B — Loxton Sands / Cross-bedding / Pata Limestone

C — Scour / Gypsum

D

E — Woorinen Fm. / Chowilla Sand / Blanchetown Clay / Upper Morgan Limestone / Jon

F — 5 cm

G — O.C. Clay / Lower Morgan Limestone

H — Silicified Sandstone / Scour / Glauconitic Sandstone / Cross-bedding / Loxton / Parilla Sands
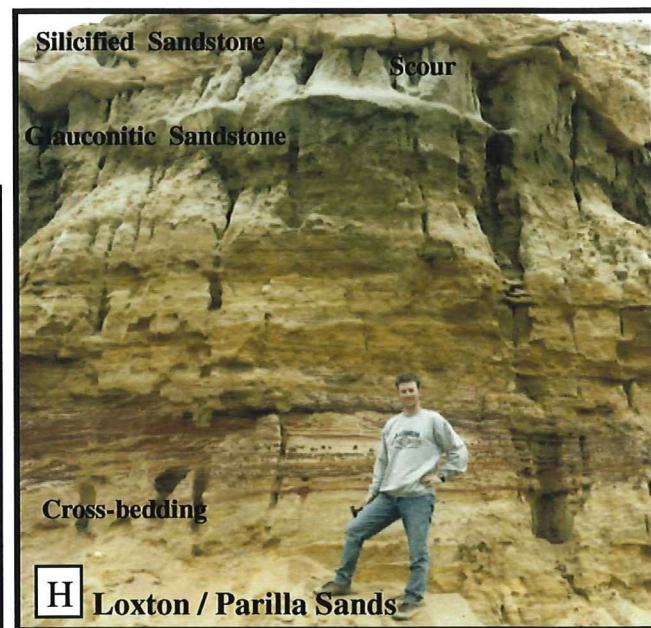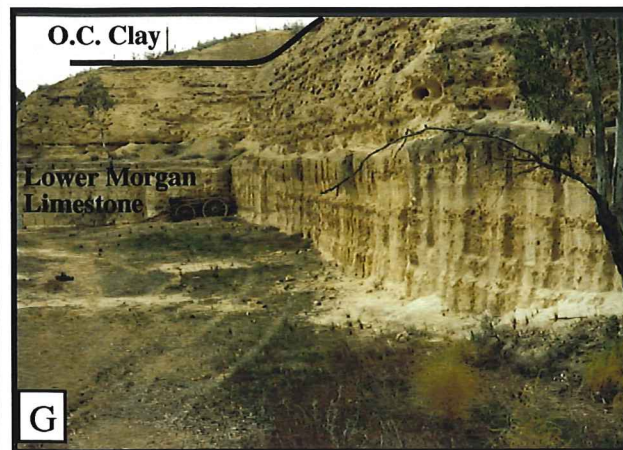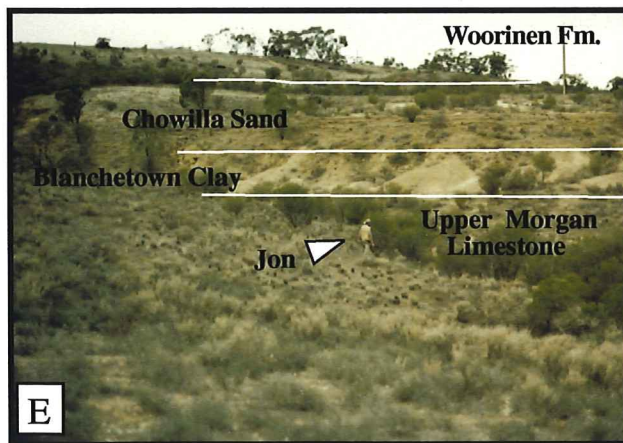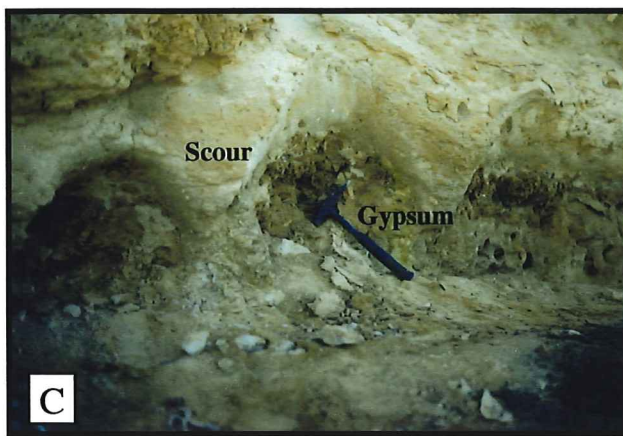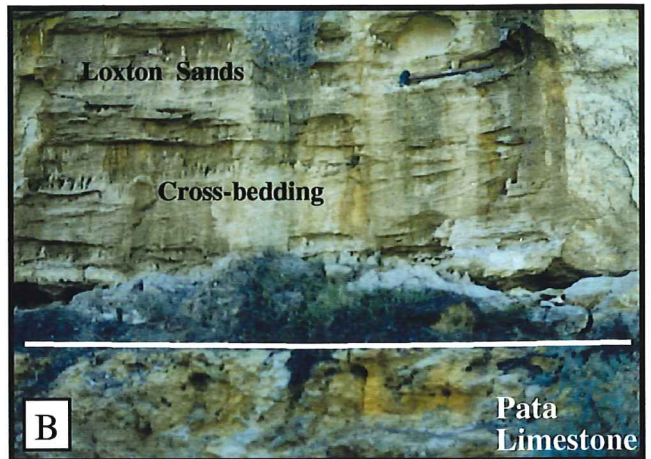
4. GEOCHEMISTRY

4.1. Introduction

Gypsum samples and representative lithologies from each locality were analysis by XRD and XRF. The results are tabulated in Appendix 11.2. Major element concentrations of whole rock and gypsum samples were determined by XRF analysis. Strontium concentrations (trace element) were determined in those gypsum samples also being analysed for Sr isotopes. Major mineralogies of samples were determined by XRD analysis. This was conducted to identify the presence of celestite ($SrSO_4$) within gypsum samples being analysed for Sr isotopes. Variation in the sodium content within gypsum may be due to fluctuations of NaCl in the groundwater. Watson (1983a) stated that fluctuations in the NaCl content of groundwaters were critical to the crystallisation of gypsum at the water table, owing to the influence of sodium salts on gypsum solubility, (figure 4.1).
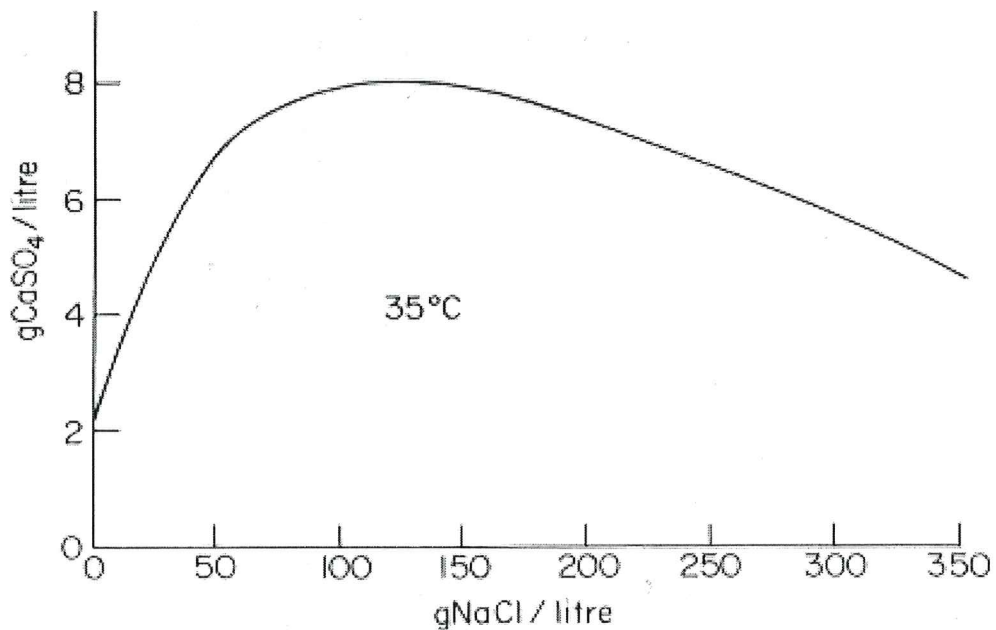
Figure 4.1. Solubility of gypsum as a function of the brine salinity, at 35°C (from Watson 1983a).

Studying Sr content in gypsum is a useful tool for interpreting the palaeosalinity of the evaporitic environments (Rosell et al. 1998), complementing isotopic and fluid inclusion analyses. The partition co-efficient of Sr, according to Halas and Krouse (1982), increases when brine concentrations rise (i.e. brine salinities are proportional to strontium content of primary gypsum). Temperature also has an effect on the partition co-efficient, but is relatively minor at temperatures below 60°C (Rosell et al. 1998). The partition co-efficient of Sr is also affected by the size and growth rate of gypsum crystals, and by the presence of celestite. Halas and Krouse (1982) stated that Sr may substitute for Ca in the crystal lattice of gypsum, forming celestite. Celestite is uncommon in gypsum containing less than 3000 ppm Sr (Rosell et al 1998), which suggests it should not be a contaminating factor within these, low Sr gypsum samples. However, it was identified within the Blanchetown Clay, where it formed a celestite nodule (figure 3.5). The gypsum nodules from this locality were not analysed for Sr. Celestite does not occur in the gypsum from Blanchetown Clay, but does occur within seed gypsum from the gypsum mine near Weston Flat (sample gyp.mine) in the Quaternary, Yamba Formation.

The presence of glauconite within the upper sandstone bed of the Loxton/Parilla Sands, at Barmera quarry, was confirmed by XRD (plate 3H). Glauconite forms in a slightly reducing environment and requires an influx of biogenic carbonate debris, as well as iron and potassium, in a moderately alkaline environment of pH 7-8 (Parron and Nahon 1981). The presence of an alkaline environment is supported by the silicification of the sandstone at the top of this bed (Plate 3.H).

The elemental proportions of samples, analysed by XRF, were recorded as the weight percent (wt.%) of their corresponding oxides. Samples were analysed for: SiO_2, Al_2O3, Fe_2O_3, MnO, MgO, CaO, Na_2O, $K2O$, TiO_2, P_2O_5 and SO_3. Initial trouble was encountered for the analysis of Ca and Mg due to an interference problem of high Ca on the Mg peak. These samples were repeated successfully after recalibrating the analytical software. However, some totals were still low, especially from samples 12.3 and 12.3.1. High Sr values in the celestite sample (12.3.1) may have been responsible for these analytical problems. Sample preparation and analytical procedures are documented in appendix 11.1. Results of major element analyses are tabulated in appendix 11.2. Strontium concentrations in gypsum range from 294 ppm to 483 ppm. These Sr concentrations are typically low for gypsum, indicating that Sr concentrations

within the parent brines were low during gypsum precipitation (Parron and Nahon 1981). The brine salinity may also have been low. The Sr content of gypsum precipitating from hyper-saline brines, is usually ~ 3000 ppm (Halas and Krouse (1982). Figure 4.3 shows the Sr content and salinity (NaCl wt% equivalent) concentration of the parent brines (determined by fluid inclusion analysis). Sodium and magnesium content of the various gypsum samples is very similar, $Na_2O\%$ 0.16 to 0.18, and $MgO\%$ 0.84 to 0.88 (Appendix 11.2). This suggests that gypsum precipitation took place within similar chemical environments.

Sr concentration vs parent brine salinity
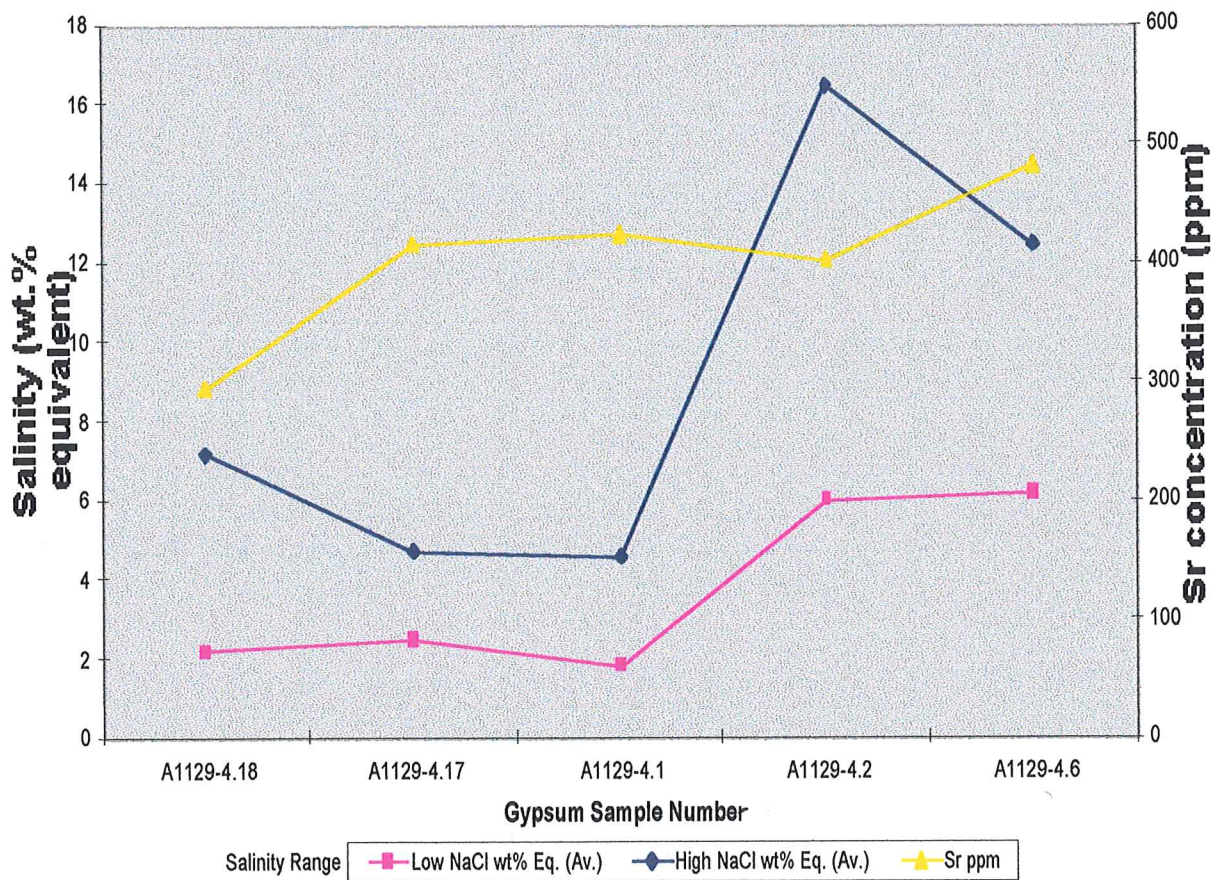
Figure 4.2. Sr verses salinity of parent brines, determined by fluid inclusion analysis. The brine salinities are recorded as NaCl equivalents, corresponding to the final melting temperature of ice within frozen fluid inclusions. The Sr concentration of gypsum should be proportional to the salinity of the parent brine, according to Halas and Krouse (1982). These results do not seem to be consistent with those of Halas and Krouse (1982). However, the large salinity ranges make a correlation difficult.

5. FLUID INCLUSIONS

5.1. Introduction

During gypsum crystal growth, small droplets of mineralizing fluid are often trapped within intracrystaline cavities. Recent and ancient gypsum samples contain fluid inclusions whose chemistries may have been altered during diagenesis. Fluid inclusions in gypsum may reflect syngenetic and diagenetic environments. Primary fluid inclusions contain original, or close to original mineralizing fluid compositions, while secondary fluid inclusions give a record of diagenetically altering waters (Attia et al. 1995). It is therefore important to be able to identify primary fluid inclusions when using them to determining the nature of the original brine. The application of simple phase diagrams (NaCl-H_2O), are used to indicate fluid salinity by the temperature of the "last melting point" of ice within a frozen fluid inclusion. Other salts (e.g. $CaCl_2$ or $MgCl_2$) may be detected by the value of the "first melting point" (Shepherd et al. 1985). Fluid inclusions can be considered primary or secondary depending on the degree of preservation of the original mineralogy, textures, and secondary structures (Attia et al. 1995).

Freezing studies are the best way to measure the salinity of aqueous inclusions. The lowering of the freezing point of pure water is directly proportional to the amount of salt in solution (Figure 5.1) (Shephered et al. 1985). Determining the salinity is achieved by measuring the final melting point of ice in a solution as the inclusion is reheated gradually from <$-100°$ C. The final melting temperature of ice will vary according to the type and concentration of salt, or salts in solution. Because the fluid composition is difficult to determine from ice melting temperatures, calculated salinities are reported as "weight % NaCl equivalents" (Shepherd et al. 1985). That is, the amount of NaCl which would produce an equivalent final melting temperature of ice.
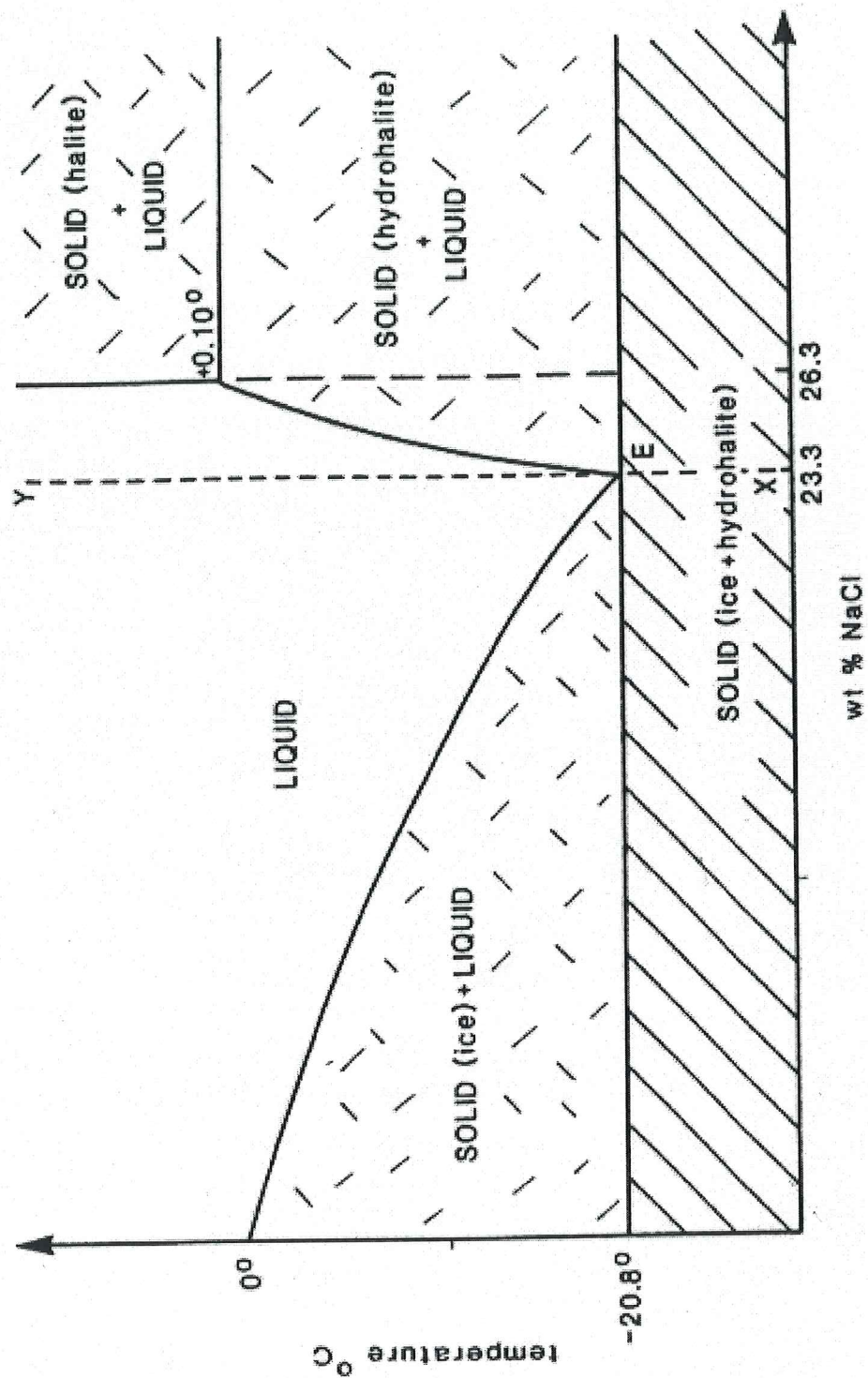
Figure 5.1 H₂O-NaCl phase diagram (from Shepherd et al. 1985). The final melting temperature of ice within a fluid inclusion can be used to calculate the salinity of the frozen solution, (recorded as weight % NaCl equivalent). The salinity of primary fluid inclusions indicate the salinity of the brine during crystal growth.

The first melting point (the first appearance of liquid, during heating) corresponds to the eutectic temperature. This is determined by the composition of the fluid (mixture of salts in the inclusion) (Eadington and Wilkins 1980). A solution containing water and NaCl will have an eutectic temperature of $-20.8°$ C. When other salts are present, the first melting temperature will change according to the type, and concentration of salts present. Figure 5.2 shows the eutectic temperatures ($°$ C) for a number of salt systems. Daughter minerals (solid phases) develop as a fluid reaches saturation point (Shepherd et al. 1985). Solid phases can often be identified by the nature of euhedral crystals, colour and isotropic birefringence.

Salt system	Eutectic Temperature ($°$ C)	Solid Phases
H_2O-NaCl-$CaCl_2$	-55.0	ice + $NaCl.2H_2O$ + $CaCl_2.6H_2O$
H_2O-MgCl-$CaCl_2$	-52.2	ice + $MgCl.12H_2O$ + $CaCl_2.6H_2O$
H_2O-KCl-$CaCl_2$	-50.5	ice + $CaCl_2.6H_2O$
H_2O-$CaCl_2$	-49.5	ice + $CaCl_2.6H_2O$
H_2O-NaCl-$FeCl_2$	-37.0	ice + $NaCl.2H_2O$ + $FeCl_2.6H_2O$
H_2O-$FeCl_2$	-35.0	ice + $FeCl_2$ + $6H_2O$
H_2O-NaCl-$MgCl_2$	-35.0	ice + $NaCl.2H_2O$ + $MgCl_2.12H_2O$
H_2O-$MgCl_2$	-33.6	ice + $MgCl_2.12H_2O$
H_2O-NaCl-KCl	-23.5	ice + $NaCl.2H_2O$
H_2O-NaCl	-20.8	ice + $NaCl.2H_2O$
H_2O-KCl	-10.6	ice

Figure 5.2. Selected phase data for salt-water systems considered most relevant to the aqueous fluid inclusions, and within the first melt temperature range recorded in this study (from Shepherd et al. 1985).

5.2. Results

A total of 287 fluid inclusions from 9 gypsum samples were examined, representing the different stratigraphic positions and gypsum forms. These samples include: the selenite layers and gypcretes from the Norwest Bend Formation and Upper Morgan Limestone, and gypsum nodules from the Overland Corner and Blanchetown Clays. Thin sections, prepared for fluid inclusion analysis were examined under the microscope and photographed. The sections were then placed in acetone to remove the gypsum from the slide. Microthermometry was used to study the freezing / melting behavior of fluid inclusions, and the temperature at which these changes took place, recorded. The observations were made at a magnification of 400x, using a fluid inclusion adapted heating / freezing stage mounted petrographic microscope. Single-phase (liquid) inclusions, two-phase (gas-liquid) and (liquid-solid) inclusions, and three-phase (gas-liquid-solid) inclusions were recognized. Vapor bubbles in some single-phase fluid inclusions were produced by freezing to -100°C, and then heated to 30°C, (causing stretching). The vapor bubbles produced in this way are in equilibrium, and were examined preferentially to other fluid inclusions. Fluid inclusions were then frozen to about -100°C, and heated at about 10°C per minute. The melting temperatures of solid phases were recorded. Slower heating rates were used near phase changes. Freezing was repeated 3-4 times or until reproducible results were obtained. Up to 5 fluid inclusions could be viewed simultaneously where the population of fluid inclusions was high. The results are recorded in figures 5.3 and 5.4, and appendix 11.2.
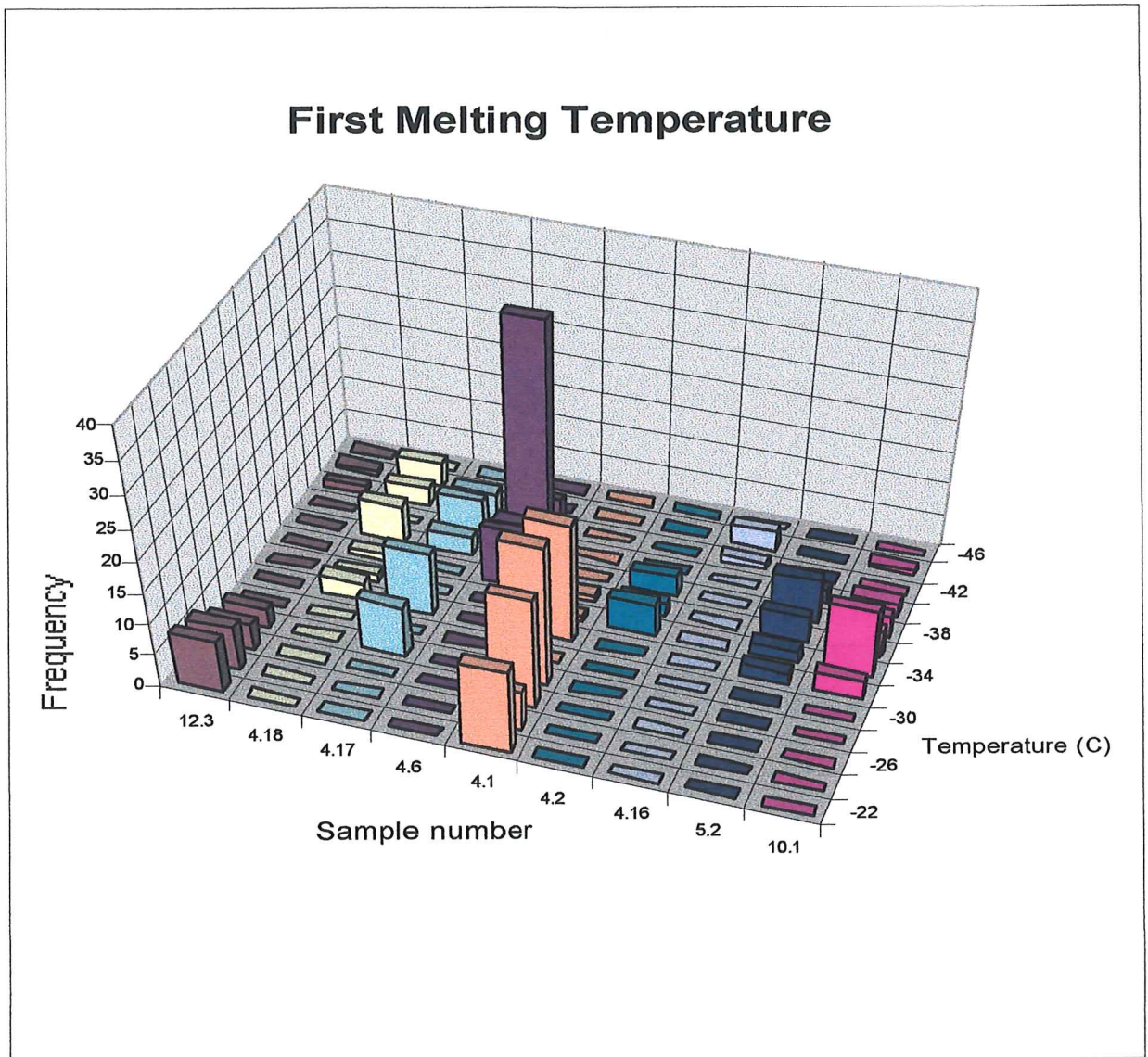
Figure 5.3. Histogram showing the first melting temperatures of ice within frozen fluid inclusions from gypsum samples. Samples 12.3 and 4.1 have high first melting temperatures, close to -21°C, indicating that NaCl is most likely the dominant salt present (refer to figure 5.2). Lower first melting temperatures suggest other salts are present within the fluid inclusions. The water-salt systems H_2O-$MgCl_2$ and H_2O-$FeCl_2$ have eutectic temperatures of −37°C and -33°C respectively. Many of the samples have melting temperatures close to these temperatures. However, the salt system $CaCl_2.6H_2O$ (with a eutectic temperature of -49.5°C), is more likely to be responsible for the lower melting points, given the composition of the host rocks.

Final Melting Temperature
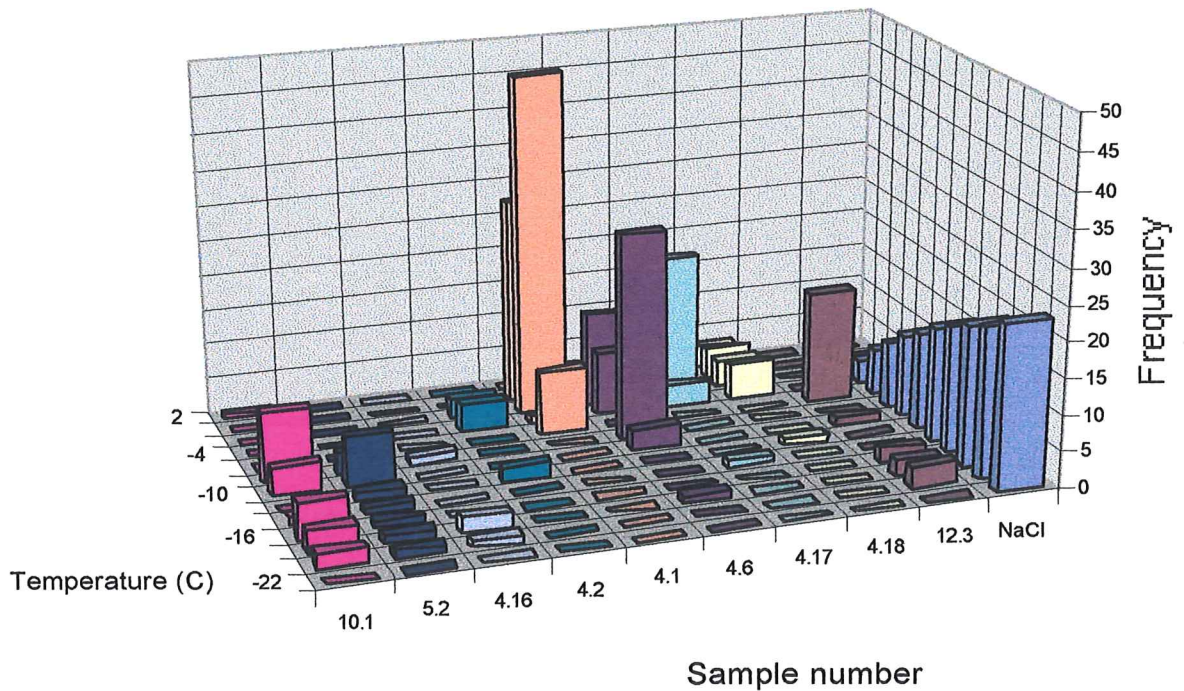
Figure 5.4. This histogram shows the final melting temperatures of ice within fluid inclusions. The height of the columns in row "NaCl", show the NaCl wt% equivalent calculated for corresponding melting temperatures (NaCl wt% is equal to the "Frequency" range values). Note that the Upper Morgan selenite (sample 4.16) and the gypsum nodules (samples 10.1, 5.2 and 12.3) have a higher, average melting point than the gypcrete samples (4.2, 4.1, 4.17). This indicates that gypsum nodules and selenite precipitated from similar, hypersaline brines. The brine responsible for gypcretes has a lower, more uniform salinity range.

The majority of fluid inclusions froze at temperatures between -40°C and -60°C, indicated by the formation of a granular appearance, which became clearer as the temperature was reduced further. Vapor bubbles generally shrank and often became irregular in shape as the liquid froze. During warming, from -100°C, the bubble often disappeared at around -76°C, but was inconsistent in its return, even within the same fluid inclusion. Bubble movements assisted in estimating first and final melts. The first melting temperatures ranged between -46°C and -21°C, with the majority between -27°C and -37°C. However, the Norwest Bend, bedded selenite sample showed consistent first melting temperatures around -21°C to -23°C. The first melting temperature was taken as the first appearance of a granular texture of ice within a fluid inclusion. This was often difficult to accurately determine, especially in the smaller fluid inclusions and fluid inclusions with only a small amount of liquid. Observations of the first melting temperatures are considered to be approximations, within 5°C of the true melting temperatures. Solid phases were identified as halite due to their cubic crystal symmetry, and pale yellow colour.

Between melting points, cracked ice crystals recrystallised to form larger rounded crystals as temperatures increased. Near the final melting temperature, ice crystals began to decrease in size, in contrast to vapor bubbles (if present). The final melting temperature of ice was taken as the instant ice was no longer visible. This phase change was usually quite easy to observe, and is therefore assumed to be very close to the actual final melting temperature. The final melting temperature of most fluid inclusions was between -10°C and -2°C. The selenite sample from the Norwest Bend Formation recorded higher final meting temperatures, between -5°C and +2°C.

An effort to distinguish between primary and secondary fluid inclusions was attempted, but once the samples were removed from the glass slide, they crumbled considerably, making their relationship to crystal boundaries and cleavages, hard to determine. An accurate determination was therefore hard to obtainable. Where a distinction could be made, it was noted (appendix 11.2). This may explain the largely bimodal distribution of final melting temperatures within the samples.

5.3. Discussion

Gypcrete and gypsum nodules most commonly precipitate from pore water within the rock or soil matrix (Bowler and Teller 1986, Ali and West 1983). Bedded selenite usually forms at the surface, within evaporite basins, where the gypsum crystals grow vertically into the saline brine from which they are precipitating (Attia et al. 1995). The salinity and salt systems present within gypsum fluid inclusions can give an indication of the likely source of the water, or mixture of waters responsible for the gypsum precipitation. The relative position of the water table during precipitation may therefore be inferred. A large variation in the ratio of liquid to vapour within fluid inclusions from the same sample indicates precipitation took place within the vadose zone (Y. Bone pers. comm. 1999). The variation in fluid inclusion salinity indicates that deposition occurred in an environment that was susceptible to environmental change. The greatest variation in salinity would occur in low volume reservoirs, such as playa lakes, or at the interface (mixing zone) of 2 different waters (e.g. the soil surface or groundwater table). In arid and semi-arid environments, such as the Murray Basin, surface and soil pore waters become increasingly saline due to evaporative concentration. Pore water salinity is susceptible to fresh, rainwater infiltration. Soil pore water may also be influenced by the upward movement of groundwater, by capillary action (figure 5.4) (Ali and West 1983). Groundwaters also mix at semi-porous confining boundaries, and with meteoric waters at the water table.

Fluid inclusions from samples recorded a first melting temperature of ice, $> -20.8°C$, except for the Blanchetown Clay gypsum nodule, where NaCl may be the only salt present. This indicates that additional salt systems to H_2O-NaCl are present in all other samples (figure 5.2). A minor amount of KCl may also be present in samples with a first melting point close to -20.8°C. However, this salt system is disregarded, as the K_2O was not detected by XRF. The additional salt/s within the other samples are most likely $CaCl_2$ in samples with a eutectic temperature of -49°C, considering the calcium rich composition of the host sediments. The salt system H_2O-$MgCl_2$ is another possibility, with a eutectic temperature of -35°C, or -33.6°C when NaCl is also present. $FeCl_2$ may also be present (eutectic temperature of -35°C), but XRF analysis of gypsum samples only detect trace amounts of Fe_2O_3 in 1 sample.
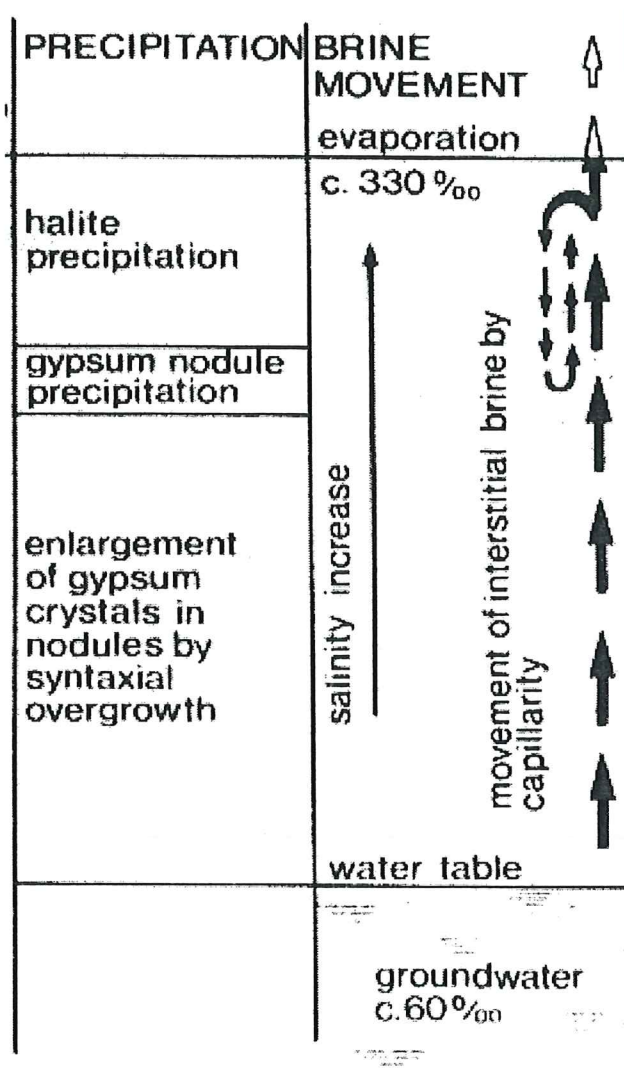
Figure 5.5. Groundwater brine movement during the arid conditions of summer, and it relationship to the sites, and type of gypsum precipitation. Comparative increases in salinity through evaporative concentration of the brine are also shown (from Ali and West 1983).

The final melting points of ice in most fluid inclusions (close to $-8°C$) indicates brine salinity concentrations, and compositions are similar to seawater evaporated to gypsum saturation point (Spencer et al. 1990). The salinity equivalents, calculated for the Norwest Bend Formation selenite, are far lower than those expected for evaporated seawater. Final melting temperatures of ice in most fluid inclusions from this sample are quite high, ranging from $-1.8°C$ to $+1.5°C$. Such high final melting temperatures suggest that at least some of the gypsum formed from relatively dilute brines. The positive melting temperatures of ice may be explained by the presence of hydro-halite. Strontium concentrations within the gypsum are proportional to the salinities interpreted from fluid inclusion studies (figure 4.2).

Plate 4.

Fluid Inclusion Photomicrographs

Plate 4.A: A number of single phase (liquid), and a 2 phase, vapour-liquid fluid inclusions in a gypsum nodule from the Blanchetown Clay, at Barmera Quarry (Sample 12.3). (x400 magnification, under plane polarised light).

Plate 4.B: An elongate, 2 phase, liquid (L) – solid (S), fluid inclusion. The daughter crystal is most likely halite given the cubic crystal symetry. From sample 12.3, a gypsum nodule from the Blanchetown Clay, at Barmera Quarry. (x400 magnification, under plane polarised light).

Plate 4.C: Two, liquid (L) – vapour (V), 2 phase fluid inclusions. The gas bubble is the gray area. Selenite from the Norwest Bend Formation (Sample 4.18). (x400 magnification, under plane polarised light).

Plate 4.D: A large, 2 phase vapour (V) – liquid (L) fluid inclusions. The cracking and reforming of ice, before finally melting was obvious in the large fluid inclusions from this sample. (x400 magnification, under plane polarised light).

Plate 4.E: A 3 phase, vapour (v) – liquid (L) – solid (S) fluid inclusion in gypcrete (sample 4.1), from the Upper Morgan Limestone, Broken Cliffs. The solid phase is most likely halite. (x400 magnification, under plane polarised light).

Plate 4.F: Parallel aligned, elongate, single phase (liquid), and 2 phase (liquid-vapour) fluid inclusion in nodular gypsum from the Upper Morgan Limestone, Sunlands Pumping Station (Sample 5.2). The dominance of vapour, and a large variation between vapour to liquid within this gypsum sample, indicates that these fluid inclusions formed within the vadose zone. The lack of growth bands suggests that they are secondary fluid inclusions. (x200, under plane polarised light).

Plate 4.G: Abundant, parallel aligned fluid inclusions within selenite, sample 4.16. (x400 magnification, under plane polarised light).

Plate 4.H: Primary fluid inclusions arranged in rows along growth zones, from selenite crystal (sample 4.16). (x400 magnification, under plane polarised light).

Plate 4.I: Growth bands within a single gypsum crystal from Broken Cliffs selenite, sample 4.11. Solid and fluid inclusions are abundant along these growth bands.

Plate 4.J: Primary fluid inclusions forming irregular bands along lineage boundaries, near the borders of crystals. Gypsum nodule from the Overland Corner Clay, at Overland Corner (Sample 10.1). (x200 magnification, under plane polarised light).

Plate 4
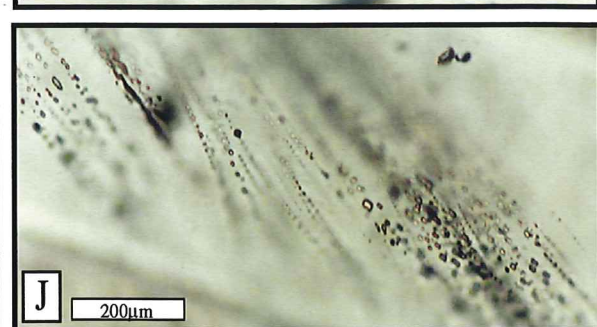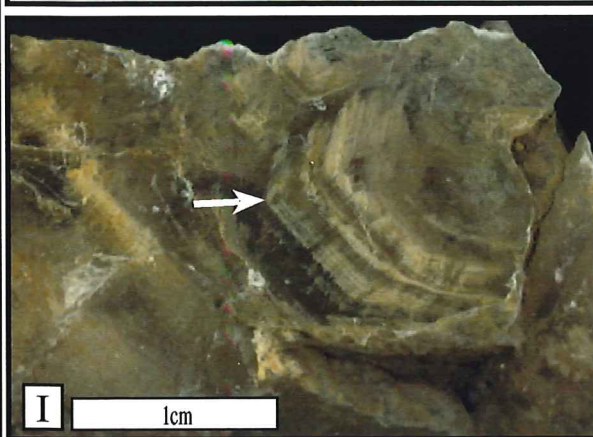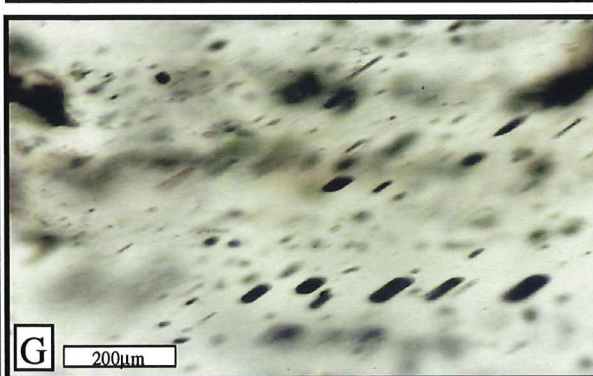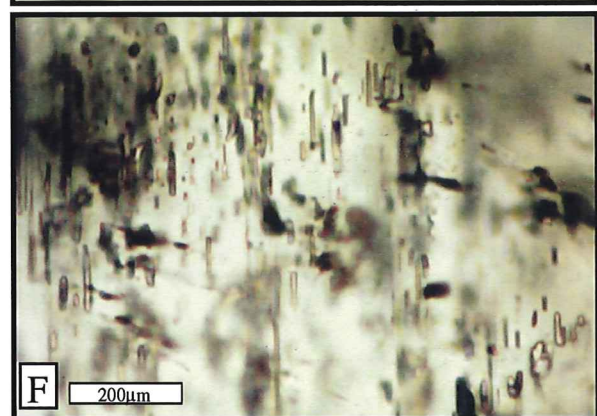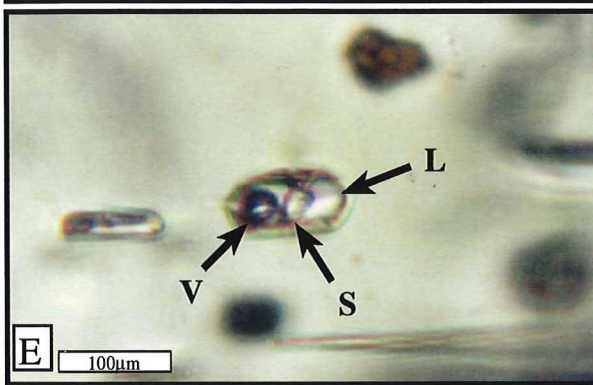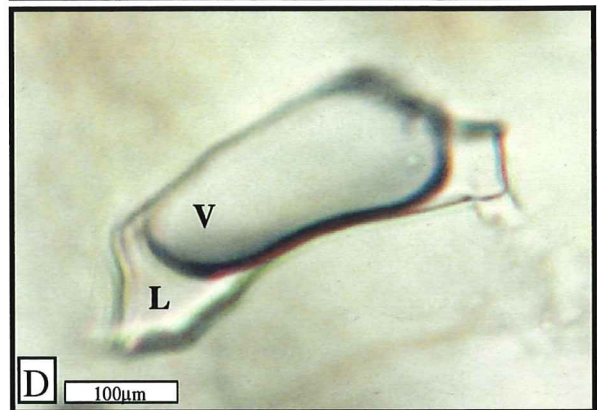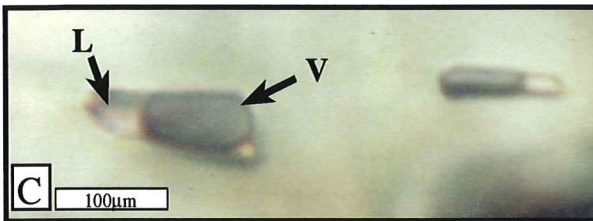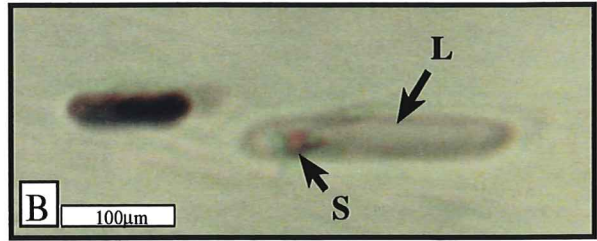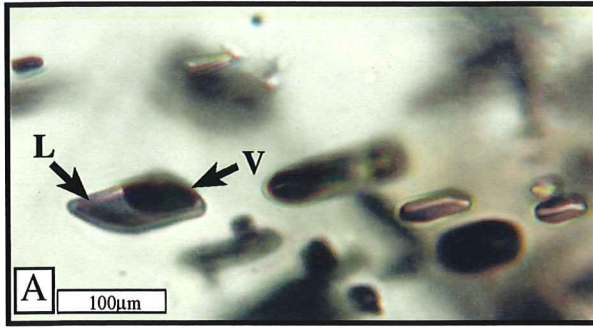
6. SULPHUR ISOTOPES

6.1. Introduction

Sulphur isotope measurements have been carried out on 16 gypsum samples, and 1 celestite sample. The main purpose of these measurements was to help establish a marine or non-marine origin for the bedded selenite, and determine the relationships between the gypsum varieties. The acquisition of at least semi-quantitative information on the palaeoenvironmental conditions during the precipitation of gypsum horizons was also anticipated. Samples representing massive, massive mesocrystalline gypsum, bedded selenite, and gypcrete were analysed. Dogramaci (1998), conducted sulphur isotope measurements on the groundwaters within the study area, in order to trace the water flow paths, and determine the amount of mixing between the confined, saline Renmark Aquifer and the unconfined, fresh Murray Group Aquifer. Kiasatpur (1999) analysed the Sulphur isotopic compositions of surface water from lagoons, creeks and the River Murray. The isotopic measurements from these previous studies are presented in figure 6.1, for comparison with the results of this study. Sample preparation and procedures for measuring the $\delta^{34}S$‰ CDT of gypsum are detailed in appendix 11.1.

Sulphur Source (sample)	$\delta^{34}S$‰ CDT	Author
Modern Seawater	+20.99‰	(Claypool et al. 1980)
Middle to Upper Miocene Seawater	+22‰	(Claypool et al. 1980)
Seed Gypsum Dune - Renmark, SA.	+16‰	(Chivas et al. 1990)
Murray Group Aquifer water (Waikerie)	+25.4‰	(Dogramaci 1998)
Murray River waters (Berri to Morgan)	+9.1‰ to +20.3‰	(Kiasatpur 1999)
Lagoons (Berri to Morgan)	+16.4‰ to +24.7‰	(Kiasatpur 1999)
Groundwater seeps	+15.7‰ to +16.1‰	(Kiasatpur 1999)
Rainwater (Berri)	+9.3‰	(Kiasatpur 1999)

Figure 6.1. Local water and gypsum $\delta^{34}S$‰ CDT measurements from other studies.

Raab at al. (1997) states the behavior of $\delta^{34}S$ in brines is dictated by:

(1) the value of $\delta^{34}S$ would only change in a marine evaporated water body in very high degrees of evaporation (the $\delta^{34}S$ value of the parent water would be preserved in the gypsum during gypsum precipitation).

(2) the $\delta^{34}S$ in gypsum, formed in the process of dolomitization, preserves the original value of the sulphur in the sulphate of the parent solution.

(3) in the process of bacterial reduction in a water body, H_2S, having a relatively low $\delta^{34}S$, is formed, resulting in a heavier sulphur in the residual sulphate solution. In the case of seawater, H_2S leaving the system will have a smaller $\delta^{34}S$ than that of the seawater. The sulphate remaining in the solution will therefore become heavier.

(4) a brine resulting from the mixing of waters of different $\delta^{34}S$ values will have an intermediate value between the end members.

6.2. Results

The isotopic values for each sample are represented in figure 6.2. The $\delta^{34}S$ values of gypsum range from +14.5‰ to +20.2‰, with the majority being +18‰ to +20‰. The lower bedded selenite layer from the Morgan Limestone at Broken Cliffs, has a $\delta^{34}S$ value of +20.2‰, which is very similar to Miocene values (Claypool et al. 1980) and present marine sulphate values, from seawater (+20.4‰) (Adelaide University Standard). The $\delta^{34}S$ values show a correlation within stratigraphic units and lithology. Within the Upper Morgan Limestone at Broken Cliffs (section 1), $\delta^{34}S$ values from both bedded selenite and gypcretes have a narrow range between +18.8‰ and +20.2‰. The Norwest Bend Formation $\delta^{34}S$ values also lie within a narrow range (+18.1‰ and +17.9‰). Gypsum from Sunlands (Upper Morgan Limestone) have $\delta^{34}S$ values of +18.0‰ and +17.9‰. Nodular gypsum from the Overland Corner and Blanchetown Clays have $\delta^{34}S$ values of +16.8‰ and +16.9‰ respectively. These 2 clay units were deposited in vastly different environments. The $\delta^{34}S$ value from the celestite nodule from the Blanchetown Clay measured +19.5‰. The lowest $\delta^{34}S$ value of +14.5‰ belongs to the seed gypsum dune (sample gyp.mine).

Figure 6.2. Gypsum δ^{34}S‰ CDT analysis.

Sulphur Source (sample)	δ^{34}S‰ CDT
Seawater standard (University of Adelaide)	+20.4‰
Seed Gypsum, near Weston Flat (Gyp.mine)	+14.5‰
Celestite, Blanchetown Clay (12.3.1)	+20.4‰
Gypsum nodule, Blanchetown Clay (12.3)	+16.9‰
Selenite, Norwest Bend Formation (4.18)	+18.1‰
Gypcrete, Norwest Bend Formation (4.17)	+19.9‰
Gypsum, karst filling, Upper Morgan (4.6)	+18.9‰
Gypcrete, Upper Morgan (4.1)	+18.8‰
Gypsum fossil fill, Upper Morgan (4.2)	+19.6‰
Gypsum crust, surface, Upper Morgan (4.8)	+19.2‰
Selenite bed (small), Upper Morgan (4.5)	+19.3‰
Selenite bed, Upper Morgan (4.11)	+20.2‰
Selenite bed, Upper Morgan (4.12)	+20.2‰
Selenite bed, Upper Morgan (4.16)	+18.0‰
Gypsum, Sunlands, Upper Morgan (5.6)	+17.9‰
Gypsum, Sunlands, Upper Morgan (5.2)	+18.0‰
Gypsum nodule, Overland Corner Clay (10.1)	+16.8‰

Figure 6.2. The δ^{34}S values of gypsum within the study area. The samples are presented in the stratigraphic order, assigned to the host unit in which they occur.

6.3. Discussion

The $\delta^{34}S$ values of non-marine water is determined by the relative contributions from rainwater, and the oxidation of pyrite minerals in catchment sediments (Raab et al. 1997). Rainwater has a relatively low $\delta^{34}S$ compared to marine water. The $\delta^{34}S$ composition of sulphate within the gypsum samples depends on a number of factors that control the $\delta^{34}S$ composition of the water from which the gypsum has precipitated. These factors relating to Murray Basin groundwaters, described by Dogramaci (1998), include:

(1) the $\delta^{34}S$ ratio of the rainwater that recharges aquifer/s contributing to the brine water.

(2) the amount of bacterial sulphate reduction in the groundwater.

(3) mineralisation of organic sulphur by bacteria in the soil.

The $\delta^{34}S$ of marine evaporites has varied over geologic time from +35‰ in the early Cambrian, +10‰ in the late Permian, to +21‰ in modern seawater (Claypool et al. 1980). Sulphur variations in continental rainfall can be attributed to by sea spray sulphate (~+21‰), biogenic aerosols (average close to 0‰), and anthropogenic sulphate which is not significant in the Murray Basin (Dogramaci 1998). Biogenic sulphur compounds contribute more to the atmospheric sulphate concentration further inland, as the effects of sea spray diminish. The $\delta^{34}S$ values of gypsum in the Australian continent are dominated by marine $\delta^{34}S$ ranging from +14‰ to +20‰ (Chivas et al. 1991). These values are generally lower than $\delta^{34}S$ values observed in the local groundwaters of the Murray Group and Renmark Group Aquifers (Dogramaci 1998).

The $\delta^{34}S$ values from the lower selenite layer from the Upper Morgan Limestone have $\delta^{34}S$ values expected for Miocene, and present seawater. The lower values found in other samples, suggest a greater influence of non-marine waters contributed to the parent brine, or subsequent altering brines. The gypcrete has similar $\delta^{34}S$ values to the bedded selenite, suggesting it may have formed from the dissolution of the selenite gypsum. This is supported by a similar $\delta^{34}S$ value of +19.2‰ from a 2mm thick gypsum crust that formed on the recently quarried cliff face at Broken Cliffs (sample 4.8) (Plate 1). This crust undoubtedly formed from the dissolution of exposed gypsum from higher up the cliff, and precipitated as the water ran down the exposed cliff face. Gypcretes, and cavity filling gypsum are possible gypsum

sources. These samples have $\delta^{34}S$ values of +18.8‰ to +19.3‰. The resultant gypsum crust has a $\delta^{34}S$ value of +19.2‰. The $\delta^{34}S$ contribution from rainwater (+9.3‰), to the crust is low.

Groundwater sulphate may have attributed to the $\delta^{34}S$ values of gypsum in many of the samples. Gypsum nodules from the Overland Corner and Blanchetown Clays have $\delta^{34}S$ values of +16.8‰ and +16.9‰ respectively. This similarity suggests that the source of these displacive gypsum nodules was similar, even though the samples are from stratigraphically different clays, of vastly different age. Seed gypsum from the working gypsum quarry, near Weston Flat, has a $\delta^{34}S$ value of +14.5‰. This is much lower than the other gypsum samples suggesting the precipitating brine was more influenced by meteoric waters. This follows the interpretation of Lockhart (1921) that these dunes originated from gypsum crusts from saline lakes. Chivas et al. (1991), and Bowler and Teller (1986), stated that $\delta^{34}S$ values of gypsum deposits of inland playas and saline lakes, depends on the relative contributions from sea-spray and rainwater.

7. STRONTIUM ISOTOPES

7.1. Introduction

The $^{87}Sr/^{86}Sr$ ratio of gypsum represents the mixed proportions of each water source to the parent brine. The $^{87}Sr/^{86}Sr$ value of the possible Sr sources is required to determine the dominant contributors. The Sr content of groundwater is initially derived from rainfall. Dissolution of Sr from minerals within the vadose, and later the phreatic zone, contributes the bulk of Sr to groundwater compositions (Dogramaci 1998). Even the $^{87}Sr/^{86}Sr$ ratio of rainwater run-off assumes an isotopic composition similar to that of the host, whole rock (Jones and Faure 1978). Therefore, the $^{87}Sr/^{86}Sr$ values of surface water and groundwater are more likely to reflect the $^{87}Sr/^{86}Sr$ ratio of the minerals within the soil and aquifer matrix, rather than the Sr input from rainfall. The $^{87}Sr/^{86}Sr$ ratio gypsum should reflect the mixed proportions of surface water and aquifer water contributing to the precipitating brine.

Strontium dissolved in rainwater is derived from sea-spray, and wind blown dust from the interior of the continent (Dogramaci 1998). Sea spray typically has a $^{87}Sr/^{86}Sr$ value similar to that of modern seawater (~0.7092), and is the main contributor to coastal rainwater (Burke et al. 1982, Hodell et al. 1990). Further inland, the contribution of marine Sr decreases significantly. Dust derived from weathering soils contributes significant amounts of alkali earth elements, about 50% of the Sr budget to inland rainwater (Chivas et al. 1990, Herut et al. 1993, Jones et al. 1993).

Strontium ions in carbonate and sulphate minerals, originating from marine water are derived from dissolved Sr in seawater. The $^{87}Sr/^{86}Sr$ ratio of seawater has varied over time, fluctuating between 0.7068 and 0.7092 over the past 600 million years (Burke et al. 1982). Miocene, $^{87}Sr/^{86}Sr$ values are very similar to present values. These variations can be used to determine the age of minerals which have precipitated from a marine derived brine (e.g. Hodel 1991, Raab et al 1997, Denison et al. 1998). The marine origin of hypersaline brines can be established by consistency of $^{87}Sr/^{86}Sr$ values from different stratigraphic levels, and growth bands from a single, laterally extensive gypsum bed, collected at separated sites (Denison et al. 1998). Determining the origin of the precipitating brine is most important as gypsum may form from marine, non-marine, or a mixture of marine and non-marine brines (e.g. Raab et al 1997). Even

if a marine origin is established, later diagenetic alteration of gypsum may modify the isotopic ratio, rendering $^{87}Sr/^{86}Sr$ values for chronology invalid.

7.2. Results

Strontium isotopes were prepared from 5 massive, crystalline gypsum samples. Three samples were from the Upper Morgan Limestone, and 2 samples from the Norwest Bend Formation at Broken Cliffs. Sampling was restricted to massive gypsum varieties where at least 1-2 grams of pure gypsum could be extracted. The large selenite bed at the base of the Broken Cliffs, and gypsum nodules were not analysed for Sr isotopes due to the high clay content along growth lines within crystals. The strontium was extracted by the ion-exchange technique by a resin mesh. The ratios were determined by a Finnigan MAT 261 multi-collector mass spectrometer, using a double collection static mode. Data blocks of ten scans were run until acceptable statistics were achieved (8-16 blocks). Procedures and the run data of samples and standards are presented in appendix 11.1.

The $^{87}Sr/^{86}Sr$ ratio of gypsum samples range from 0.7106 to 0.7110, with the highest value being from the gypcrete within the Norwest Bend Formation (sample 4.17). Gypsum samples from the Upper Morgan Limestone have a slightly lower $^{87}Sr/^{86}Sr$ ratio. The contribution of Sr from silicate minerals, which have $^{87}Sr/^{86}Sr$ ratios ranging between 0.7014 and 0.7201, may be attributing to the isotopic value in samples from the Norwest Bend Formation. The original marine minerals within the Murray Group limestones retain a marine, (Miocene) $^{87}Sr/^{86}Sr$ value (0.7085), (Hodel et al. 1991, Dogramaci 1998). Dissolution of these minerals by meteoric water may have contributed a small amount of Sr to the gypsum, lowering its $^{87}Sr/^{86}Sr$ ratio slightly from that of the silicate minerals. Gypsum samples from the Morgan limestones have slightly lower $^{87}Sr/^{86}Sr$ ratios than gypsum from the Norwest Bend Formation. The ratios vary slightly, ranging from 0.7106 (sample 4.6) to 0.7108 (sample 4.1). The $^{87}Sr/^{86}Sr$ ratios of each sample are shown in figure 7.1.

Sample	Sr concentration	$^{87}Sr/^{86}Sr$
4.18	0.294 ppm	0.710574
4.17	0.415 ppm	0.711024
4.1	0.424 ppm	0.710768
4.2	0.402 ppm	0.710657
4.6	0.483 ppm	0.710596
Blank (av.)	(wt. 2167 pg)	±0.00002

Figure 7.1. The $^{87}Sr/^{86}Sr$ ratio of gypsum samples range from 0.7106 to 0.7110. Sample 4.17, a gypcrete from the oyster beds of the Norwest Bend Formation, has a higher $^{87}Sr/^{86}Sr$ ratio than the samples from the Upper Morgan Limestone. This may be due to a higher contribution of Sr from silicate minerals, with $^{87}Sr/^{86}Sr$ ratios ranging between 0.7014 and 0.7201 (Dogramaci 1998). These values are considerably higher than $^{87}Sr/^{86}Sr$ ratio of ancient and modern seawater (0.7085 to 0.7092).

7.3. Discussion

Rainwater entering surface sediments quickly assume a similar $^{87}Sr/^{86}Sr$ value to the sediments they are infiltrating (Jones and Faure 1978). This is due to the low Sr content of rainwater becoming inundated by the Sr within the sediments (Raab et al. 1997). In the Murray Basin, at Broken Cliffs, the surface sediments are the sandstones and oyster beds of the Norwest Bend Formation. The infiltrating water would therefore assume $^{87}Sr/^{86}Sr$ values similar to that of the silicates (~0.7111). As the water continues downward, entering the Upper Morgan Limestones, the $^{87}Sr/^{86}Sr$ ratio would gradually change, eventually assuming $^{87}Sr/^{86}Sr$ ratios similar to that of the limestones (~0.7085). The change in the $^{87}Sr/^{86}Sr$ ratio of meteoric water, as it pass through the vadose zone, are recorded by the gypsum that precipitated from it (Denison et al. 1998). The $^{87}Sr/^{86}Sr$ ratio of gypsum samples from the Upper Morgan

Limestone, at Broken Cliffs is very similar to the $^{87}Sr/^{86}Sr$ ratio of silicate minerals that dominate the Norwest Bend Formation. The likely contributors to the $^{87}Sr/^{86}Sr$ ratio of gypsum varieties are shown in figure 7.2.
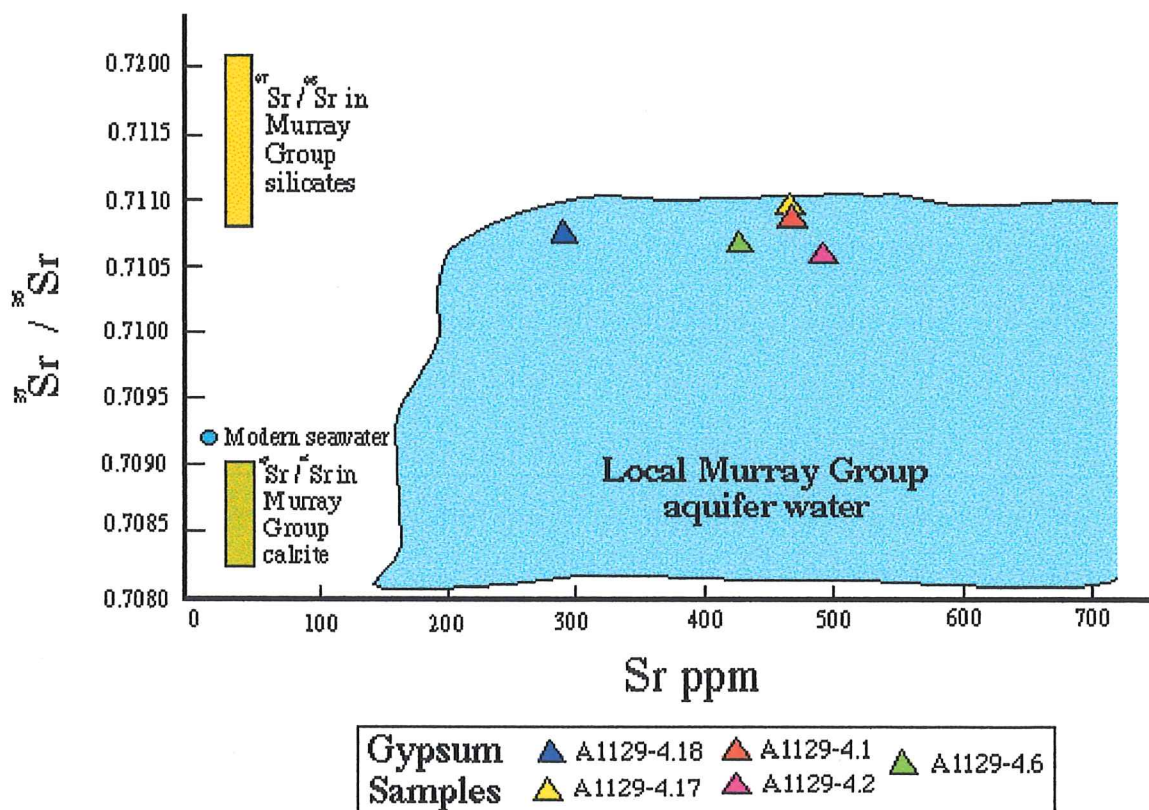
Figure 7.2. The $^{87}Sr/^{86}Sr$ ratio of possible Sr contributors to gypsum varieties within the Murray Basin.

8. SUMMARY

The chemical and morphological diversity exhibited by the gypsum forms indicates a variety of genetic processes. Gypsum crystallisation from evaporating surface waters is discounted for the formation of gypsum crusts, on the grounds of the high clastic content. This indicates that the gypsum accreted within the host sediment. The large crystal size and poikilitic inclusions of host rock grains suggest that crystallization took place under stable hydro-chemical conditions, allowing uninterrupted crystal growth. Large gypsum crystals develop in the alluvial zone, since evaporation is slower, allowing longer periods for ionic migrations to growing crystal faces (Watson 1983a). Stable brine conditions are supported by the analytical data, also indicating sub-surface precipitation. The salinity of the brines fluctuated only slightly (0 to 6 wt% NaCl equivalent), compared to the salinity of the brines precipitating selenite and nodular gypsum. The Sr concentrations of the gypcretes are consistent, and low (402 to 415 ppm), also an indication of low brine salinity (figure 7.1). The aeolian gypsum deposits may have been the initial sulphate source for the formation of these, sub surface crust. Deflation of recent evaporite minerals from dry lake beds is suggested to be a major vector for gypsum crust formation. This abundant source is likely to have contributed, but sulphur isotopes from recent gypsum dunes have a much lower, meteoric $\delta^{34}S$ value (+14.5‰), than the gypcretes (~+19‰). The primary sulphur source must have a lower $\delta^{34}S$ value. Local groundwater, from the Murray Group Aquifer, has a $\delta^{34}S$ value of ~ +25‰. The upward movement of groundwater to the surface by capillary action or the elevation of the groundwater table may be contributing the $\delta^{34}S$ of gypsum crusts. The $\delta^{34}S$ of the gypsum seem to be influenced by its proximity to the water table (perceived as a stratigraphic correlation). Sulphur isotopes from selenite and nodular gypsum also have close to marine $\delta^{34}S$ values. Rising groundwater transports dissolved gypsum to the surface where it precipitates (Bowler and Teller 1986). The contribution of marine $\delta^{34}S$, from the dissolution of marine minerals from limestone, may also increase with depth. However, gypsum hosted by stratigraphically lower limestones, but further from the water table has a higher $\delta^{34}S$ value (sample 5.2, from Sunlands).
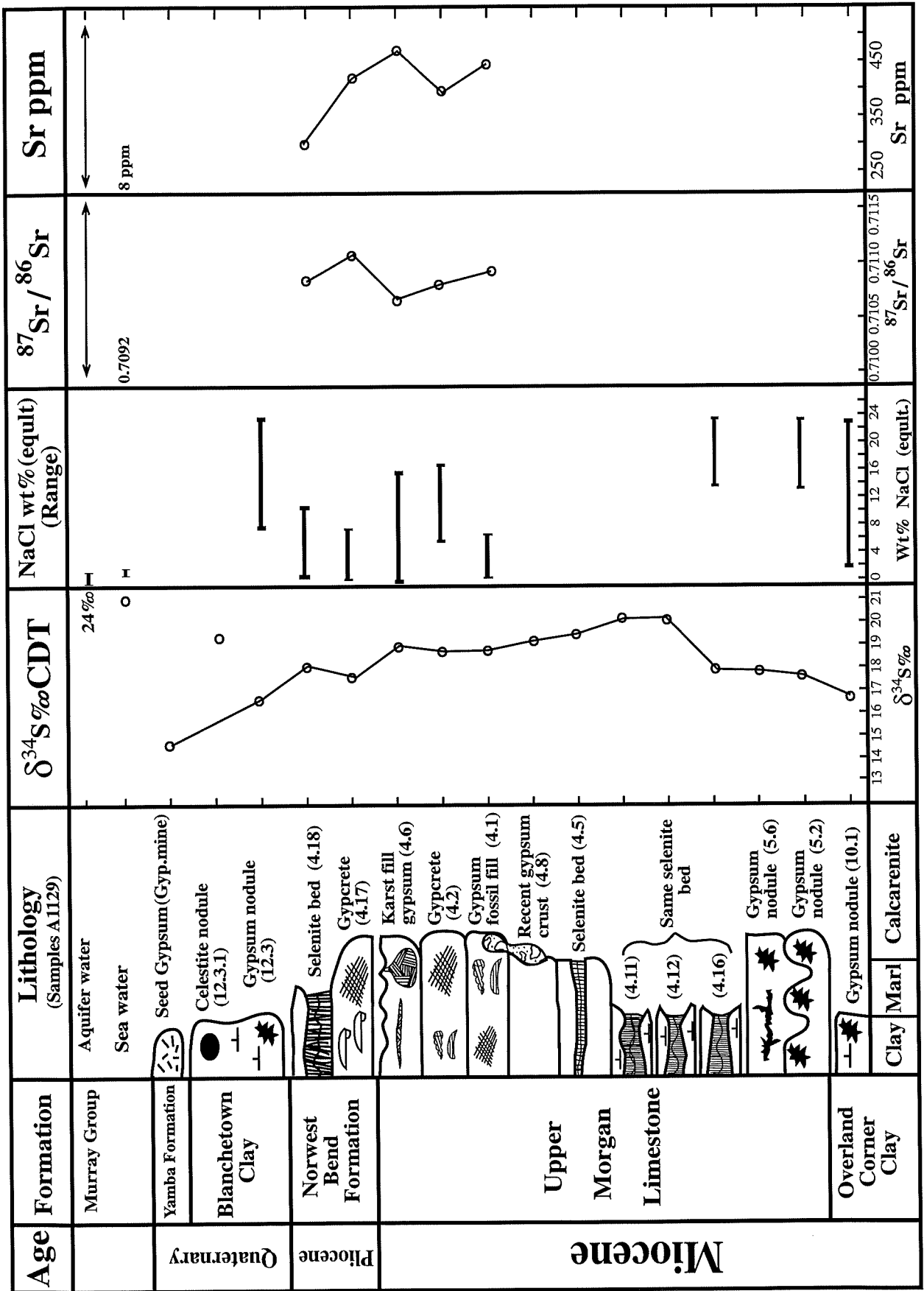
Figure 8.1 Relative stratigraphy of gypsum samples and analytical results.
(B. P. Thomas 1999)

43

Growth fabrics of bedded selenite within the Norwest Bend Formation, and the Upper Morgan Limestone, suggest gypsum precipitated from a standing body of water. Precipitation in such environments takes place at the brine-sediment interface, growing upward into the brine, forming vertically orientated crystals with horizontal growth bands defined by solid and fluid inclusions (Plates 2.H and 4.I). The trapping of mud along detrital partings in the bedded selenite, suggest that the inflow water carrying the detrital material, may have already been saturated with gypsum (Attia et al. 1995). If the selenite beds did precipitate from an open body of water, they would have an age equivalent to the host rocks. This is unlikely to be the case given. The smaller selenite bed occurs within a homogeneous calcarenite, which shows no signs of a break in sedimentation where it lenses out.

Gypsum nodules exhibit similar crystal morphologies and chemistries to selenite, indicating they may have formed in similar environments with fluctuating salinities. Fluctuation in the salinity of groundwater facilitates gypsum precipitation (Watson 1983a, Ali and West 1983). As meteoric water, low in NaCl, but high in $CaSO_4$ recharges saline groundwater, the solubility of gypsum may be reduced sufficiently to cause gypsum to precipitate (figure 4.1). High sodium content in brines has been suggested to influence the development of gypsum crystals. Edinger (1973) stated that the adsorption of sodium ions on the (111) crystal face retards growth at the expense of the (102) face. This causes the development of lenticular gypsum crystals precipitating from hyper saline brines. The selenite layers, and the core of gypsum nodules exhibit lenticular crystal habits (Plate 3.F). Salinities, interpreted from fluid inclusion analysis, indicate the brine responsible for gypsum nodules and selenite crystals was hyper saline. The brine responsible for massive, crystalline gypsum crusts was relatively dilute (figure 7.1). Salinity variations in fluid inclusions within a single selenite bed vary considerably, indicating that water salinities fluctuated during crystal growth. Salinity fluctuates the greatest where water of different salinities mix. The low first melting temperatures (<-20.8°C) of ice in fluid inclusions indicates that the fluids contain more than 1 chloride salt, in addition to NaCl. Calcium chloride, with a eutectic temperature of -49°C, is most likely the additional salt, considering the composition of the host rocks. Strontium contents of gypsum reflect the high salinities interpreted from fluid inclusion studies.

The upward displacement of host sediment grains is the most likely method of selenite, and gypsum nodule formation. Moisture held by surface tension against grain boundaries

evaporates from the surface down, causing crystallisation of gypsum at grain contacts (Keen 1936). The unidirectional growth of gypsum crystals may achieve a pressure of $4000kN/m^2$, equivalent to 20-25 m of dry quartz sand (Goudie et al. 1970). Crystal growth initiates at grain boundaries, when interstitial pore moisture is available. Subsequent crystal growth occurs at contacts between crystal boundaries, displacing them, rather than increasing their size (Watson 1983a). The growth bands exhibited by the selenite layers and gypsum nodules may have formed by this form of displacive crystallisation. Since this form of gypsum crystallisation is associated with evaporation of pore waters, it is most likely restricted to the near surface and along cliff exposures.

9. CONCLUSIONS

The formation of gypsum crusts and selenite beds in the western Murray Basin, can be explained by the movement of gypsum bearing groundwater. The infiltrating meteoric water is diverted by thin, less porous clay layers. Water moving laterally along these layers, seeps out where the layer intersects the cliffs along the Murray River. Evaporative concentration near the surface causes gypsum to precipitate in hypersaline conditions. Crystal growth occurs at contacts between crystal boundaries, causing the lateral displacement of the host sediment. Subsequent crystal growths trap inclusions of host rock, forming a horizontal layering. The high salinity of the brine water is the main control on gypsum crystal habit, producing lenticular to fibrous crystals. Gypsum nodules formed in much the same way as the selenite layers. They are probably small broken segments of eroded selenite beds that formed at the top of the impermeable clay layer. The prismatic crystals on surrounding the nodules are most likely caused by the partial dissolution of gypsum by infiltrating meteoric water. Evaporation of this less saline water results in the reprecipitation of prismatic gypsum crystals around the perimeter of a lenticular selenite core (Plate 3.F). The $^{87}Sr/^{86}Sr$ ratios of the gypsum crusts indicate they are derived from the dissolution of the aeolian gypsum dunes. Precipitation of these gypcretes took place below the surface in stable brine conditions. Gypsum from upward moving groundwater, by capillary action, is unlikely to have contributed to gypsum crust given their topographic position, with respect to the water table.

The formation of these gypsum layers is dependent on the evaporation of groundwater as it seeps out of the host sediments along the base of the Murray River cliffs. This assigns the deposits a maximum, Pleistocene age (~0.6 Ma) to gypsum formation, post dating the draining of Lake Bungunnia, and the formation of the Murray River Gorge. Lake Bungunnia covered a large portion the central Murray Basin between 2.5 Ma and 0.7 Ma. The demise of the megalake indicated the onset of aridity in Southern Australia. Salt lakes, responsible for the aeolian gypsum dunes, may have directly descended from Lake Bungunnia.

10. REFERENCES

ABELE, C., 1976. Introduction to the Tertiary. *In:* Douglas, J. G. and Ferguson, J. A. (Eds). *Geology of Victoria. Geological Society of Australia,* Special Publication 5: 177-191.

ABELE, C., 1988. Introduction to the Tertiary. *In:* Douglas, J. G. and Ferguson, J. A. (Eds). *Geology of Victoria. Geological Society of Australia,* Special Publication: 251-265.

ALI, Y. A. AND WEST, I., 1983. Relationships of modern gypsum nodules in sabkhas of Loess to compositions of brines and sediments in Northern Egypt. *Journal of Sedimentary Petrology,* 53 (4): 1151-1168.

ATTIA, O. E., LOWENSTEINE, T. K. and WALI, A. M. A., 1995. Middle Miocene gypsum, Gulf of Suez: marine or non-marine? *Journal of Sedimentary Research,* 65 (4), 614-626.

BLACKBURN, G., 1962. Stranded coastal dunes in North-western Victoria. *Australian Journal of Earth Science,* 388-389.

BOWLER, J. M. AND TELLER, J. T., 1986. Quaternary evaporites and hydrological changes, Lake Tyrrel, north-west Victoria. *Australian Journal of Earth Sciences,* 33:43-63.

BROWN, A., 1984, Effects of depth, depositional texture, and clay content on porosity loss in ancient limestones. *In:* The Geological Society of America, South, Central Section, 18th annual meeting: Abstracts with Programs. *Geological Society of America,* 16 (2): 79.

BROWN, C. M. & STEPHENSON, A. E., 1986. Murray Basin, southeastern Australia: Subsurface Stratigraphic Database. *Bureau of Mineral Resources,* Report 262.

BROWN, C. M. & STEPHENSON, A. E., 1991, Geology of the Murray Basin, southeastern Australia: Bureau of Mineral Resources. *Geology and Geophysics,* Bulletin 235.

BROWN, C. M., 1985. Murray Basin, southeastern Australia: Stratigraphy and resource potential - a synopsis. *Bureau of Mineral Resources,* Report 264.

BROWN, C. M., 1988, Overview of the geology of the Murray Basin. *In:* Murray Basin Abstracts, Geology, Groundwater and Salinity Management Conference, 1988. *Bureau of Mineral Resources, Geology and Geophysics,* 12: 23-30.

BURKE, W. H., DENISON, R. E., HETHERINGTON, E. A., KOEPNIK, R. B., NELSON, H. F. AND OTTO, J. B., 1982. Variation of seawater $^{87}Sr/^{86}Sr$ throughout Phanerozoic time. *Geology,* 10: 516-519.

CLAYPOOL, G. E., HOLSER, W. T., KAPLAN, I. R., SAKI, H. AND ZAK, I, 1980. The age curves of sulphur and oxygen isotopes in marine sulphate and their mutual interpretation. *Chemical Geology,* 28: 199-260.

CHIVAS, A. R., ANDREW, A. S., LYONS, W. B., BIRD, M. L. AND DONNELLY, T. H., 1991. Isotopic constraints on the origin of salts in the Australian Playas. 1. Sulphur. *Palaeogrophy, Palaeoclimatology, Palaeoecology,* 84: 309-332.

CRESPIN, I., 1944. The occurrence of Cycloclypeus in the Tertiary deposits of South Australia. *Transactions of the Royal Society of South Australia,* 68 (1): 120-121.

DENISON, R. E., KIRKLAND, D. W. AND EVANS, R., 1998. Using Strontium Isotopes to determine the Age and Origin of Gypsum and Anhydrite Beds. *The Journal of Geology,* 106: 1-17.

DOGRAMACI, S, S., 1998. Isotopes of Sulphur, Oxygen, Strontium and Carbon in groundwater as tracers of mixing and geochemical processes, Murray Basin, Australia. *PhD thesis, University of Adelaide, Adelaide (unpublished).*

EADINGTON, P. J. AND WILKINS, R. W. T., 1980. The origin, interpretation, and chemical analysis of fluid inclusions in minerals. *Technical communications 69, Institute of Earth Resources, CSIRO, 1-23.*

EDINGER, S. E., 1973. An investigation into the factors which effect the size and growth rates of the habit facies of gypsum. *Journal of Crystal Growth*, 18: 217-224.

FIRMAN, J. B., 1965. Late Cainozoic lacustrine deposits in the Murray Basin, South Australia. *Quaternary Geological Notes, Geological Survey of South Australia*, 16.

FIRMAN, J. B., 1973. Regional stratigraphy of surficial deposits in the Murray Basin and Gambier Embayment. *Geological Survey of South Australia, Report of Investigations*, 39.

GEISLER, C. D., 1987. Strontium and bromine, salinity indicators from Recent evaporitic deposits (salt marshes) and fossil deposits (Triassic Messinian). *In*: Sassi, S. (Ed.), *International Association of Sedimentologists 8th regional meeting of Sedimentology*. International Association of Sedimentology Regional Meeting, 8:240-241.

GILES, S. D., 1972. Stratigraphic investigations of Tertiary sequences, Western Murray Basin, South Australia. *Honours Thesis, University of Adelaide, Department of Geology and Geophysic, Adelaide (unpublished)*.

GILL, E. D., 1973. Geology and Geomorphology of the Murray River Region between Mildura and Renmark, Australia. *National Museum of Victoria, Memoirs*, 34: 1-99.

GOUDIE, A., COOKE, R. U. AND EVANS, I., 1970. Experimental investigation of rock weathering by salts. *Area*, 4: 42-48.

HALAS, S. AND KROUSE, H. R., 1982. Isotopic abundance of water of crystallization of gypsum from the Miocene evaporite formation, Carpathian, Foredeep, Poland. *Geochemica et Cosmochimica. Acta*, 46: 293-296.

HARRIS, P. M., 1985a. Carbonate cementation, a brief review. *In:* Schneiderman, N. and Harris, P. M., (Ed). Carbonate cements. *Society of economic paleontologists and mineralogists*, Special publication 36: 79-97.

HARRIS, W. K., 1966. New and redefined names in South Australian lower Tertiary stratigraphy. *Geological Survey of South Australia, Quarterly Geological Notes*, 20: 1-3.

HARRIS, W. K., 1985b. Middle to Late Eocene depositional cycles and dinoflagellate zones in southern Australia. In: Lindsay, J. M., (Ed). Stratigraphy, Palaeontology, Malacology. *Papers in Honour of Nell Ludbrook. Department of Mines and Energy, South Australia.* Special Publication No.5: 133-144.

HERUT, B., STARINSKY, A. AND KATZ, A., 1993. Strontium in rainwater from Israel: Sources, isotopes and chemistry. *Earth Planet Science Letters*, 231: 979-984.

HILLS, E. S., 1939. The Physiography of Victoria. *Royal Society of Victoria, Proceedings*, 51: 175-194.

HODELL, A. D., MEAD, A. G. AND MUELLER, A. P., 1990. Variations in strontium isotopic composition of seawater (8 Ma to present): implications for chemical weathering rates and dissolved fluxes to the oceans. *Chemical Geology*, 80: 291-307.

HOWCHIN, E., 1929. Notes on the geology of the Great Pyap Bend, River Murray, and remarks on the history of the River Murray. *Royal Society of South Australia, Transactions*, 53: 167-195.

JACK, R. L., 1921. The salt and gypsum resources of South Australia. *Geological Survey of South Australia, Bulletin*, 8: 118.

JONES, L. M. AND FAURE, G., 1978. A study of the strontium isotopes in lakes and surficial deposits of the ice-free valleys, South Victoria Land, Antarctica. *Chemical Geology*, 22: 107-120.

JONES, F. B., HANOR, J. S. AND EVANS, W. R., 1993. Sources of dissolved salts in the central Murray Basin, Australia. *Chemical Geology*, 111: 135-154.

KEEN, B. A., 1936. The circulation of water in soil between the surface and the level of underground water. *Bulletin of the International Association of Scientific Hydrology.* 22: 328-331.

KIASATPUR, G,. 1999. Geochemical study of the salinity and pollution of groundwater and surface-waters in the Murray Basin, Renmark to Morgan, South Australia. *Honours thesis, University of Adelaide, Adelaide (unpublished).*

KOTSONIS, A., 1995. Late Cainozoic climate and eustatic record from the Loxton - Parilla Sand, Murray Basin, South Australia. *Unpublished Masters Thesis, School of Earth Sciences, University of Melbourne.*

LAWRENCE, C. R., 1966. Cainozoic Stratigraphy and Structure of the Mallee Region, Victoria. *Royal Society of Victoria, Memoir,* 30.

LAWRENCE, C. R., 1973. Geology, Hydrodynamics and Hydrogeochemistry of the Southern Murray Basin. *Geological Survey of Victoria, Memoir,* 30: 1.

LINDSAY, J. M. and BARNETT, S. R., 1989. Aspects of stratigraphy and structure in relation to the Woolpunda Groundwater Interception Scheme, Murray Basin, South Australia. *Bureau of Mineral Resources. Journal of Australian Geology and Geophysics,* 11: 219-225.

LINDSAY, J. M. and BONNETT, J. E., 1973. Tertiary stratigraphy of three deep boreholes in the Waikerie area of the Murray Basin. *Geological Survey of South Australia, Report of Investigation,* 38.

LINDSAY, J. M. and WILLIAMS, A. F., 1977. Oligocene marine transgression at Hartley and Monarto, southwestern margin of the Murray Basin. *Geological Survey of South Australia, Quarterly Geological Notes,* 64, 9-16.

LOCKHART, J. R., 1921. Papers - Underground water in South Australia. Salt and Gypsum Resources South Australia. *South Australian Department of Mines, Geological Survey of South Australia.* Bulletin 8: 83-118.

LUDBROOK, N. H., 1961. Stratigraphy of the Murray Basin in South Australia: *Geological Society of South Australia,* Bulletin 36.

LUDBROOK, N. H., 1963. Correlation of the Tertiary rocks of South Australia. *Royal Society of South Australia, Transactions,* 87: 5-15.

LUKASIK, J. J. AND JAMES, N. P., 1998. Lithostratigraphic revision and correlation of the Oligo-Miocene Murray Supergroup, western Murray Basin, South Australia. *Australian Journal of Earth Science,* 45: 889-902.

MACPHAIL, M. K., KELLETT, J. R., REXILIUS, J. P. AND OÍRORKE, M. E., 1993. The "Geera Clay Equivalent": a regressive marine unit in the Renmark Group that sheds new light on the age of the Mologa weathering surface in the Murray Basin. *Journal of Australian Geology and Geophysics,* 14: 47-63.

McGOWRAN, B., 1979. The Tertiary of Australia: Foraminiferal overview. *Marine Micropalaeontology,* 4: 235-264.

MUCUMBER, P. G., 1969. The inland limits of the Murravian marine transgression in Victoria. *Australian Journal of Science,* 32: 165-166.

MUCUMBER, P. G., 1978. Evolution of the Murray River during the Tertiary Period: evidence from Northern Victoria. *Royal Society of Victoria, Proceedings,* 90: 43-52.

O'DRISCALL, E. P. D., 1960. The Hydrology of the Murray Basin Province in South Australia. *Geological Survey of South Australia,* Bulletin 35.

PARRON, C. AND NAHON, D., 1981. Red bed genesis by lateritic weathering of glauconite sediments. *Journal of the Geological Society,* 137: 689-694.

QIANYU, L. AND MCGOWRAN, B., 1999. Miocene foraminifera from the Finniss Clay and Cadell Marl, western Murray Basin: taxonomic and taphonomic contrasts and their environmental significance. *Alcheringa,* 23: 133-152.

QIANYU, L. AND MCGOWRAN, B., 1999. Miocene foraminifera from the Finniss Clay and Cadell Marl, western Murray Basin: taxonomic and taphonomic contrasts and their environmental significance. *Alcheringa,* 23: 133-152.

RAAB, M., FRIEDMAN, G. M., SPIRO, A., STARINSKY AND ZAK, I., 1997. The geological history of Messinian (Upper Miocene) evaporites in the central Jordan Valley (Israel) and how strontium and sulphur isotopes relate to their origin. Carbonates and Evaporites, 12 (2): 296-324.

ROGERS, P. A., LINDSAY, J. M., ALLEY, N. F., BARNETT, S. R., LABLAK, K. L. AND KWITKO, G., 1995. Murray Basin. *In:* DREXEL, J. F. AND PREISS, W. V. (Ed). *The geology of South Australia, Volume 2, The Phanerozoic,* 157-163. Department of Mines and Energy South Australia, Bulletin 54.

ROSELL, L., ORTI', F., KASPRZYK, E., PLAYA' AND PERYT, T. M., 1998. Strontium geochemistry of Miocene primary gypsum: Messinian of southeastern Spain and Sicily and Badenian of Poland. *Journal of Sedimentary Research,* 68 (1): 63-79.

SCHREIBER, B. C., ROTH, M. S. AND HELMAN, M. L., 1982. Recognition of primary facies characteristics of evaporites and the differentiation of these forms from diagenetic overprints. *In:* Handford, C. R., Loucks, R. C. and Davies, G. R. (Ed). Depositional and Diagenetic Spectra of evaporites - A core workshop. *SEPM Core Workshop,* 3: 1-32.

SHEPHERD, T. J., RANKIN, A. H. AND ALDERTON, D. H. M., 1985. *A practical Guide to Fluid Inclusion Studies.* Blackie and Sons, London.

SPENCER, R. J., MOLLER, N. AND WEARE, G. H., 1990. The prediction of mineral solubilities in natural waters: a chemical equilibrium model for the Na-K-Ca-Mg-Cl-SO$_4$-H$_2$O system at temperatures below 25°C. *Geochemica et Cosmochimica Acta,* 54: 575-590.

SPRIGG, R. C., 1952. The Geology of the South-East Province, South Australia, with Special Reference to Quaternary Coastline Migrations and Modern Beach Developments. *Geological Survey of South Australia,* Bulletin 29.

STEPHENSON, A. E., 1986. Lake Bungunnia: a Plio-Pleistocene megalake in Southern Australia. *Paleogeography, Palaeoclimatology and Palaeoecology,* 57: 137-156.

THOMAS, B., BONE, Y. AND CLARKE, J., 1999. Fossil whale bones in the Middle Miocene Glenforslan Formation, Morgan. *Mines and Energy South Australia Journal,* 15: 32-33.

THORNTON. R. C. N., 1974. Hydrocarbon potential of Western Murray Basin and infrabasins. *In:* Report of investigations. *Geological Survey of South Australia,* 41.

THORNTON. R. C. N., 1976. Murray Basin and associated infrabasins. *In:* Leslie, R. D., Evans, H. J. and Knight, C. L., (Ed). Economic Geology of Australia and Papua New Guinea, Volume 3: Petroleum. *Australasian Institute of Mining and Metallurgy, Melbourne, Monograph Series,* 7: 91-94.

TICKELL, S. J. AND HUMPHRYS, W. G., 1979. The Geology of the Riverine Plain in Victoria. *Geological Survey of Victoria, Report, 1979/135.*

TWIDALE, C. R., LINDSAY, J. M. AND BOURNE, J. A., 1978. Murray Valley Gorge in South Australia: age and origin. *Geological Society of Victoria, Proceedings,* 90: 27-42.

WATSON, A., 1983a. Gypsum Crusts. *In:* Goudie, A. S. and Kenneth, P. (Ed). *Chemical Sediments and Geomorphology,* 5: 133-161.

WATSON, A., 1983b. Evaporite sediments in non-marine environments. *In:* Goudie, A. S. and Kenneth, P. (Ed). *Chemical Sediments and Geomorphology,* 6: 163-185.

WATSON, A., 1985. Structure, chemistry and origins of gypsum crusts in the southern Tunisia and central Namib Desert. *Sedimentology,* 32: 855-875.

11. APPENDICES

11.1 Methods

X-Ray Diffraction Measurement

Powders of whole rock and acid treated samples were ground using a mortar and pestle with distilled water to form a slurry. The slurry was placed on two thirds of a glass slide to make a smear mount. The analysis was done using Cobalt k α radiation of wavelength 1.7902$\approx$ on a Philips PW1050 diffractometer with graphite monochromator. The samples were run over the 2° range of 30-38° at 1/2° per minute with 0.01° increments. JCPDS Manuals were used in the identification of minerals. The mole percent of magnesium carbonate was calculated using an Mg calc. basic computer program. The computer program compares the distance between quartz and carbonate peaks to that of pure carbonate crystal displacings, derived from Graf (1961) and Goldsmith et al. (1961).

X-Ray Fractionation Measurement

Preliminary sample preparation: The samples were crushed with a sledge hammer to gravel sized pieces and milled for a short time in a W_2C (tungsten carbide) mill vessel, to produce a fine powder for analysis.

Major elements: The powders were dried in an oven for 2 hours to remove the absorbed moisture. They were then weighed into alumna crucibles and ignited overnight in a furnace at 960°C, to yield the Loss On Ignition (LOI) values. This comprises organic material, CO_2 from carbonate minerals, H_2O^+ (water combination with crystal structure), and possibly S, Cl and other volatiles, depending on the mineralogy of the sample. Nominally 1g of the ignited material was then accurately weighed with 4g of flux (commercially available as type 12:22, comprising 35.3% lithium tetrborate and 64.7% lithium metaborate). The sample-flux mix

was fused using a propane-oxygen flame, at a temperature approx. 1150°C, using Pt-Au crucibles, and cast into a preheated mould to produce a glass disc suitable for analysis.The samples were analysed using a Philips PW 1480 Xray Fluorescence Spectrometer, using an analysis program calibrated against several international and local Standard Reference Materials (SRM's). A dual-anode (Sc-Mo) Xray tube was used at 40kV, 75m≈.

Results: The results are presented on a "dry basis" in tabular form as oxides, the traditional form for silicate analysis. The analyses are on the "whole" sample, including any organic material that may be present. The iron is analysed as total Fe (combining the ferrous and ferric forms), expressed as Fe_2O_3. The method is suitable for silicates, but had some initial trouble analysisng the "extreme" compositions in some limestone and gypsum samples. The trouble seemed to be an interference problem of the high Ca on the Mg peek. These samples were repeated after recalibrating the software, however some totals were still low, especially for samples 12.3 and 12.3.1, which were later identified as celestite ($SrSO_4$) from XRD. The software was calibrated for carbonates at the time of analysis.

The oxides analysed are: SiO_2, Al_2O3, Fe_2O_3, MnO, MgO, CaO, Na_2O, K2O, TiO_2, P_2O_5, SO_3.

Trace elements: About 5-10g of sample powder was mixed with 1ml of binder solution (Poly Vinyl Alcohol) and pressed to form a pellet. This was allowed to dry in air and was heated for a further 1 to 2 hours in a 60°C over to ensure that the pellet was completely dry before analysis. The samples were analysed using a Philip PW 1480 XRF Spectrometer, using analysis programs suited for optimizing Strontium analysis. The programs are calibrated against several international and local Standard Reference Materials (SRM's). The duel-anode Sc-Motube operated at sufficient voltage to excite Mo, and an Au tube was use for the analyses. Matrix corrections are made using either the Compton Scatter peak, or mass absorption coefficients calculated for the major element data.

Results: The results are presented as elements in tabular form, expressed as ppm. The detection limit is 3ppm. Only Strontium has been analysed as a trace element from various gypsum samples.

Sulphur Isotopes Measurement

Sulphur isotope analysis was undertaken on approximately 25μg of sample which had been crushed and dried in a drying oven at 180°C overnight. Fine grained, silt contaminated gypsum samples were not prepared for strontium isotopic analysis, but they were analysed for sulphur isotopes. Powders of these samples were placed in 1 molar HCl overnight to dissolve the carbonate constituent, increasing the samples gypsum percentage (slightly) in order to obtain a larger sample of SO2 gas, without removing gypsum. The samples were mixed with approximately 110μg of Cu_2O and 210μg of SiO_2 powders using a mortar and pestle. The mixed powders were then placed in an open ended glass tube and plugged with silica wool. SO_2 gas was extracted, isolated, and collected on vacuum lines by using near freezing ethanol to remove water, and liquid nitrogen to remove carbon dioxide. Near freezing n-pentane was used to isolate the sulphur dioxide while carbon dioxide was being removed. Liquid nitrogen was then used to freeze sulphur dioxide into sample tubes. Samples were then measured for isotopic ratio on a Micromass VG 602E mass spectrometer with dual collector and Europe Scientific Isotope Ratio Measurement program (#5003 IRMS).

Fluid Inclusion analysis

Representative samples of bedded and massive selenite from the Broken Cliffs and Sunlands Pumping Station cliff sections were collected. Fluid inclusion slides were prepared, polished to approximately 70 microns. The slides were examined under the microscope for the size, shape, abundance, and distribution of fluid inclusions, and photographed before being placed in acetone overnight to remove the samples from the slide. Microthermometry was used to study the freezing/melting behavior of fluid inclusions; and the temperatures at which these changes took place recorded. The observations were made at a magnification of 400x, using a fluid inclusion adapted microscope adapted for a gas flow heating/freezing stage mounted petrographic microscope. One-phase (liquid) inclusions, two-phase (gas-liquid) and (liquid-solid), and three-phase (gas-liquid-solid) inclusions were recognised. Vapour bubbles in some single-phase liquid inclusions produced vapor bubbles by freezing to -100°C (causing stretching), and then heating to 30°C. The vapour bubbles produced in this way are in equilibrium, and were examined preferentially to the originally 2 phase inclusions (Attia et al.

1995). Fluid inclusions were then frozen to about -100°C, then heated at about 10°C per minute and the melting temperatures of solid phases recorded. Slower heating rates were used near phase disappearances. The freezing run was repeated 3 to 4 times (or until reproducible results were obtained) on each field of view (up to 5 inclusions simultaneously). The final melting temperatures enable calculation of fluid salinities and therefore that of the parent brine solution using the temperature-composition diagram from Shephards et al. (1985).

Strontium Isotope analysis

Five gypsum samples were analysed for ^{87}Sr / ^{86}Sr ratios. 1g of sample powder was dissolved in distilled HCl and evaporated in Teflon vessels. It was then redissolved in HCl and centrifuged in order to separate any undissolved precipitate. The strontium was extracted by the standard cation-exchange column procedure. The purified Sr^{2+} was converted to nitrate form and taken up in 30µl of 0.15 M H_3PO_4, and loaded onto a single tantalum (Ta) filament for the mass spectrometer measurements. The ratios were determined by a Finnigan MAT 261 multicollector Mass Spectrometer. 8-15 data blocks of 10 scans were run until consistent results were obtained. A value of 0.70±0.00002 was received for the standard material (Spike B), Sr Av. blank, 2167 pg.

11.2 APPENDICES

RESULTS / TABLES

XRD   Analysis   Results

Stratigraphic Unit	Sample (A1129)	Dominant	Sub-dominant	Minor / Significant	Minor (trace)	Trace
Bryants Creek	4.1	Gypsum		Dolomite	Quartz	
Broken Cliffs	4.2	Calcite	Dolomite	Gypsum	Quartz	
"	4.5	Gypsum			Dolomite	Quartz, Kaolinite, Magnetite?
"	4.5al	Gypsum			Quartz	Kaolinite, Amphibole?
"	4.11	Gypsum			Quartz, Kaolinite	Kaolinite
"	4.12	Gypsum		Dolomite, Halite	Quartz	
"	4.12al	Gypsum		Dolomite	Quartz	
"	4.16	Gypsum			Magnetite	Quartz, Kaolinite
"	4.16al	Gypsum			Quartz	Kaolinite
Bryants Creek	5.2	Gypsum				Magnetite, mica, quartz
Sunlands Pump	5.2al	Gypsum				Feldspar, Quartz, Magnetite
Station						
"	5.2ac	Bassanite				Quartz, Feldspar, others?
"	5.6	Gypsum	Calcite	Halite, Quartz	Kaolinite	Dolomite?
"	5.6al	Gypsum			Quartz, Magnetite	Kaolinite, Dolomite?
Overland Corner	10.1	Gypsum			Magnetite	Quartz
Clay						
Overland Corner	10.1al	Gypsum			Magnetite	Quartz, Mica
"	10.2ac	Quartz		Kaolinite,	Halite, Smectite, Illite, Calcite	Dolomite, Gypsum
Loxton Sands	12.2	Quartz		Glauconite	Feldspar	
Barmera Quarry	12.3	Gypsum				Magnetite, Quartz, Others?
"	12.3al	Gypsum				Magnetite, Quartz, Others?
"	12.3.1	Celestite				Quartz, Geothite
"	12.3.1al	Celestite				Quartz, Geothite
Seed Gypsum	gypmine.al	Gypsum			Quartz	Celestite, Magnetite
near Weston Flat	gypmine	Gypsum			Quartz	Celestite, Magnetite

X R F   A N A L Y S I S

Location/Fm	Sample	SiO2%	Al2O3%	Fe2O3T%	MnO%	MgO%	CaO%	Na2O%	K2O%	TiO2%	P2O5%	SO3%	LOI%	Sr ppm	Total
BC NWB	4.18 gyp	0.21	0.16	0	0	0.88	38.83	0.17	0	0.03	0.07	56.7	3.35	294	100.4
BC NWB	4.17 gyp	0.02	0.01	0	0	0.85	38.89	0.18	0	0.04	0.07	56.51	4	415	100.57
BC Morgan L	4.6 gyp	0.01	0	0	0	0.84	38.17	0.16	0	0.04	0.07	55.44	5.11	483	99.84
BC Morgan L	4.1 gyp	0.02	0	0.01	0	0.85	38.86	0.17	0	0.04	0.07	56.41	3.51	424	99.94
BC Morgan L	4.2 gyp	0.02	0.01	0	0	0.84	38.46	0.17	0	0.04	0.07	55.89	4.54	402	100.04
Westn Fl Yam. F	gyp.mine	8.75	0.47	0.22	0.03	0.99	36.66	0.27	0.06	0.08	0.08	53.61	2.21	NR	103.39
Barn Q BlanchC	12.3	2.34	0.72	0.32	0	0.87	39.31	0.25	0.09	0.07	0.07	57.85	2.7	NR	104.6
Barn Q BlanchC	12.3.1	2.21	0.46	0.17	-0.02	0.32	-0.19	0.13	0.08	-0.02	0.04	20.52	0.81	NR	24.5
BC Morgan L	4.1	6.38	0.97	1.19	0.05	8.42	32.52	0.25	0.04	0.09	0.07	29.27	21.3	NR	100.57
BC Morgan L	4.2	91.2	3.42	1.26	0	0.43	0.06	0.47	0.93	0.2	0.01	0	1.69	NR	99.67
BC Morgan L	4.5	5.98	1.18	0.96	0.01	2.94	34.3	0.42	0.07	0.14	0.07	46.3	11.33	NR	104.35
BC Morgan L	4.11	2.32	0.77	0.36	0.01	0.84	36.99	0.45	0.08	0.07	0.07	54.24	8.46	NR	104.65
BC Morgan L	4.12	6.09	0.7	0.94	0.01	9.11	26.52	4.31	0.15	0.06	0.27	21.94	23.15	NR	93.26
BC Morgan L	4.16	3.52	1.08	0.7	0.01	2.38	38.26	0.25	0.1	0.09	0.07	52.71	5.19	NR	104.38
Sunl.PS Morg L	5.2	4.04	1.32	0.66	0	0.96	37.61	0.31	0.11	0.11	0.07	55.39	3.37	NR	104.96
Sunl.PS Morg L	5.6	12.31	2.21	1.29	0.01	1.79	23.13	9.53	0.22	0.11	0.08	7.74	26.07	NR	84.48
OCCnr. OC Clay	10.1	1.93	0.58	0.27	0	0.85	37.79	0.43	0.05	0.07	0.07	58.55	2.41	NR	105.03

Westn Fl Yam. F	-	(near)	Weston	Flats	Yamba	Formation
Barn Q & BlanchC	-	Barmera	Quarry	Blanchetown	Clay	
BC NWB	-	Broken	Cliffs	Norwest	Bend	Formation
BC Morgan L	-	Broken	Cliffs	Upper	Morgan	Limestone
Sunl.PS Morg L	-	Sunlands	Pumping	Station	Upper	Morgan Limestone
OCCnr. OC Clay	-	Overland	Corner	Overland	Corner	Clay

FLUID INCLUSION ANALYSIS

Thirty fluid inclusions, examined from nodular gypsum from the Overland Clay (sample 10.1), gave a first melting temperature range between -46°C to -32°C, with an average of -35°C. The variations do not vary outside the inaccuracy estimation for first melt recordings. The bimodal trend in final melting temperatures of ice is likely to be real. Final melting temperatures ranged from -23°C to +2.4°C, with the 2 mode averages being -8.5°C, and -17°C. One 3 phase (gas-liquid-solid) fluid inclusion was observed, containing 2 small, yellow, cubic halite crystals which reformed as 1 larger crystal after the first freezing run. This fluid inclusion had an unusual final melting temperature of +2.4°C.

The first melting temperature for ice in the lowest bedded selenite layer, from the Upper Morgan Limestone at Broken Cliffs (Section 3, sample 4.16), ranged between -42°C and -44°C with an average of -43.5°C. Final melting temperatures ranged between -8°C and -21°C with an average of -16°C. The final melt temperature spread seems to be bimodal. However, this trend cannot been established as there are too few data points (4). This was due to the majority of the fluid inclusions observed showing no change during freezing or heating runs.

The first melting temperature for fluid inclusions within nodular gypsum from the Upper Morgan Limestone at Sunlands Pumping Station (sample 5.2) ranged from -40°C to -32°C, with an average of -36°C. Final melting temperatures ranged from -8°C to -21°C. These temperatures tend toward a bimodal distribution, with the average of each being -9°C and -16°C. However, only 5 fluid inclusions out of the 17 observed contribute to the lower average.

The first melting temperature of 79 fluid inclusions from kast filling, mesocrystaline gypsum from the Upper Morgan Limestone at Broken Cliffs (sample 4.6), ranged from -33°C to -37°C, with an average of -36°C. Final melting temperatures ranged from -8°C to +2.2°C. These temperatures tend toward a bimodal distribution, with the average of each being -9°C and -4°C.

Nine fluid inclusions were analysed from the pseudomoph gypsum (fossils), from the Upper Morgan at Broken Cliffs, Section 1 (sample 4.2). The first melting temperatures ranged between –38˚C and -31˚C, with an average of -34˚C. Final melting temperatures range between –12˚C and +2.2˚C, with an average of -5.4˚C.

Eighty three fluid inclusions were analysed from the gypcrete within the Upper Morgan at Broken Cliffs, Section 1 (sample 4.1). Most fluid inclusions were clear, elongate and aligned sub-parallel the a prominent cleavage plane, and are interpreted as being primary fluid inclusions. The first melting temperatures ranged between –37˚C and -22˚C, with an average of -27˚C. Final melting temperatures had a narrow range of –2.7˚C and +0.7˚C, and an average of -1.4˚C.

Thirty fluid inclusions were analysed from the gypcrete within the Norwest Bend Formation at Broken Cliffs, Section 3 (sample 4.17). The first melting temperatures ranged between –42˚C and -31˚C, with an average of -36˚C. Final melting temperatures had a wide range of –8˚C and +5.2˚C. This range was due to 2 outliers. Excluding these 2 fluid inclusions, a narrow range of –2.7 and +0.8, with an average of -2.2˚C.

Nineteen fluid inclusions from the Norwest Bend bedded selenite layer at Broken Cliffs, section 3 (sample 4.18) have a first melting temperature ranging between -31°C and -47°C. These results are tending toward a bimodal distribution with averages of -40.5°C and -32°C. The final melting points ranged between -5°C and +2°C.

The first melting temperature for fluid inclusions within nodular gypsum from the Blanchetown Clay at Barmera Quarry (sample 12.3) ranged from -21°C to -46°C and averaged -24°C. Two anomalous values had considerably lower first melting points than the majority of fluid inclusions (-42°C and -46°C). Final melting temperatures have a range of -5°C to -29°C, and show a bimodal distribution, with the average of each mode being -5.5°C and -17°C.

Appendix 11.2 Fluid Inclusion Data

Local/ Strat. Unit	Sample	Total Area of Inclusion	Total Area of Bubble	% Area Bub/Inc.	Phase	First Melt (T.*C)	Last Melt (T.*C)	Satinity (wt%NaCl Eq.)	Comments Daughter Min., Size, Shape, melt T
Barmera Quarry	12.3	650	0.0	0.0	1	-22	-5.5	8.55	
Blanchetown Clay	12.3	72	0.0	0.0	1	-23	-6	9.21	
	12.3	45	0.0	0.0	1	-23	-5.8	8.95	
	12.3	35	0.0	0.0	1	-23	-5.5	8.55	
	12.3	55	0.0	0.0	1	-22	-6	9.21	
	12.3	120	0.0	0.0	1	-23	-6	9.21	
	12.3	145	0.0	0.0	1	-22	-6	9.21	
	12.3	255	0.0	0.0	1	-21	-5.8	8.95	
	12.3	180	17.3	9.6	2	-28	-5.1	8	smooth ice from -16
	12.3	130	0.0	0.0	1	-22	-5.9	9.08	
	12.3	70	0.0	0.0	1	-23	-5.1	8	
	12.3	35	0.0	0.0	1	-21	-5.9	9.08	
	12.3	30	0.0	0.0	1	-21	-5.8	8.95	
	12.3	65	0.0	0.0	1	-22	-6	9.21	
	12.3	120	0.0	0.0	1	-23	-5.6	8.68	
	12.3	85	0.0	0.0	1	-23	-5.8	8.95	
	12.3	62	24.0	38.7	2	-25.5	-16	19.45	
	12.3	40	6.0	15.0	2	-25	-15	18.63	
	12.3	40	32.0	80.0	2	-25	-17	20.22	
	12.3	75	17.3	23.0	2	-42	-9	12.85	smooth ice from- 21
	12.3	130	7.0	5.4	2	-46	-29	23.18	bubble goes at 3 back at -75
	12.3	110	0.0	0.0	1	-28	-19	21.68	all grey
	12.3	36	0.0	0.0	1	-26.5	-18.5	21.33	all clear
	12.3	36	0.0	0.0	1	-28	-19	21.68	all grey
	12.3	30	6.0	0.0	2				N/A
	12.3	32	0.0	0.0	1				N/A
	12.3	15	4.0	26.7	2				N/A

	12.3	84	0.0	0.0	1				N/A
	12.3	30	5.1	0.0	2				N/A
	12.3	8	0.0	0.0	1				N/A
Broken Cliffs	4.18	1500	180.0	12.0	2	-47	-11.5	15.47	angular, irregular, grey, appeared about -40, melted -27
Norwest Bend	4.18	24	3.0	12.5	2	-43	1.5	0	
	4.18	60	4.0	6.7	2	-44	1.6	0	
	4.18	170	16.0	9.4	2	-42	-4.5	7.17	bubble back +1.8
	4.18	96	0.0	0.0	1	-44	1.8	0	smooth ice -13
	4.18	21	2.0	9.5	2	-42	-4.1	6.59	
	4.18	24	3.4	14.3	2	-42	-4.7	7.45	bubble back +1.8
	4.18	36	13.7	38.1	2	-37	-4.2	6.74	
	4.18	10.5	3.0	28.6	2	-38	-0.9	1.57	smooth ice from-13
	4.18	12	4.0	33.3	2	-38	-1	1.74	smooth ice from-13
	4.18	18	5.0	27.8	2	-38	-0.8	1.4	smooth ice from-13
	4.18	14	4.0	28.6	2	-38	-0.9	1.57	smooth ice from-13
	4.18	22	7.0	31.8	2	-38	-0.5	0.88	smooth ice from-13
	4.18	30	3.4	11.4	2	-36	-4.1	6.59	
	4.18	34	0.0	0.0	1	-32	-1.3	2.24	
	4.18	60	40.0	66.7	2	-32	-1.7	2.9	
	4.18	56	0.0	0.0	1	-31	-1.8	3.06	
	4.18	60	0.0	0.0	1	-34	-1.8	3.06	smooth ice from-13
	4.18	210	0.0	0.0	1				N/A
Broken Cliffs	4.17	912	0	0.0	1	-40	-2.9	4.8	
Norwest Bend	4.17	1120	120	10.7	2	-42	-3.1	4.96	
	4.17	860	0	0.0	1	-37	-2.9	4.8	
	4.17	140	0	0.0	1	-40	-2.9	4.8	
	4.17	1240	0	0.0	1	-37	-2.7	4.49	
	4.17	480	0	0.0	1	-40	-1.8	3.06	
	4.17	960	0	0.0	1	-42	-1.2	2.07	
	4.17	720	0	0.0	1	-37	-1.5	2.57	
	4.17	820	0	0.0	1	-42	-1	1.74	
	4.17	940	0	0.0	1	-40	-2.4	4.03	
	4.17	320	0	0.0	1	-40	-1.1	1.91	
	4.17	2500	36	1.4	2	-41	5.2	0	
	4.17	450	45	10.0	2	-40	-13	16.89	

	4.17	28	0	0.0	1	-32	-1.8	3.06
	4.17	120	0	0.0	1	-32	-1.8	3.06
	4.17	120	0	0.0	1	-32	-1.8	3.06
	4.17	120	0	0.0	1	-31	-3.1	5.11
	4.17	220	0	0.0	1	-27	-3.2	5.26
	4.17	210	0	0.0	1	-27	0.8	0
	4.17	240	0	0.0	1	-31	-2.5	4.18
	4.17	320	0	0.0	1	-32	-2.5	4.18
	4.17	140	0	0.0	1	-32	-2.5	4.18
	4.17	440	0	0.0	1	-32	-2.5	4.18
	4.17	360	0	0.0	1	-27	-2.5	4.18
	4.17	344	0	0.0	1	-28	-2.5	4.18
	4.17	288	0	0.0	1	-27	-2.5	4.18
	4.17	142	0	0.0	1	-27	-2.5	4.18
	4.17	120	0	0.0	1	-32	-2.5	4.18
	4.17	380	0	0.0	1	-27	-2.5	4.18
	4.17	360	0	0.0	1	-27	-2.5	4.18
	4.17	236	0	0.0	1	-32	-2.5	4.18
Broken Cliffs	4.1	36	4.0	11.1	2			N/A
Upper Morgan	4.1	27	0.0	0.0	1			N/A
	4.1	3	0.5	15.0	2			N/A
	4.1	3	0.8	26.7	2			N/A
	4.1	6	1.0	16.7	2			N/A
	4.1	91	0	0.0	2	-33	-2.2	3.71
	4.1	80	0	0.0	1	-36	-2.1	3.55
	4.1	64	2	3.1	2	-32	-2.4	4.03
	4.1	80	4	5.0	2	-34	-3.1	5.11
	4.1	68	0	0.0	1	-27	-2.2	3.71
	4.1	112	0	0.0	1	-27	-2.2	3.71
	4.1	150	4	2.7	2	-33	-2.2	3.71
	4.1	40	4	10.0	2	-33	-1.8	3.06
	4.1	440	6	1.4	2	-28	-2	3.39
	4.1	124	0	0.0	1	-29	-2.1	3.55
	4.1	140	0	0.0	1	-29	-2	3.39
	4.1	160	0	0.0	1	-28	-1.8	3.06
	4.1	100	0	0.0	1	-32	-2.2	3.71

4.1	80	0	0.0	1	-29	-2.3	3.87
4.1	90	0	0.0	1	-27	-2.4	4.03
4.1	88	0	0.0	1	-33	-2.2	3.71
4.1	480	360	75.0	2	-32	-6.6	9.98
4.1	64	2	3.1	2	-32	-0.4	0.71
4.1	140	12	8.6	2	-27	-0.8	1.4
4.1	148	4	2.7	2	-33	-2.2	3.71
4.1	80	0	0.0	1	-33	-0.4	0.71
4.1	66	0	0.0	1	-28	-2.2	3.71
4.1	48	0	0.0	1	-29	-1.8	3.06
4.1	240	0	0.0	1	-29	-1.2	2.07
4.1	48	5	0.0	2	-33	-0.8	1.4
4.1	70	2	0.0	2	-28	0.4	0
4.1	80	0	0.0	1	-29	-0.4	0.71
4.1	220	0	0.0	1	-29	-0.8	1.4
4.1	420	2	0.0	2	-28	-0.7	1.23
4.1	200	12	0.0	2	-32	-0.4	0.71
4.1	68	6	8.8	2	-33	-2.2	3.71
4.1	120	0	0.0	1	-28	-1.8	3.06
4.1	124	0	0.0	1	-29	-1.2	2.07
4.1	88	0	0.0	1	-29	-0.8	1.4
4.1	90	0	0.0	1	-28	-2.5	4.18
4.1	64	0	0.0	1	-32	0.7	0
4.1	480	0	0.0	1	-33	-1.8	3.06
4.1	64	0	0.0	1	-28	-1.2	2.07
4.1	140	0	0.0	1	-29	-0.8	1.4
4.1	148	4	2.7	2	-29	-2.5	4.18
4.1	80	4	5.0	2	-28	0.7	0
4.1	66	0	0.0	1	-32	-1.8	3.06
4.1	48	0	0.0	1	-27	-1.2	2.07
4.1	240	0	0.0	1	-33	-0.8	1.4
4.1	48	6	12.5	2	-32	-0.7	0
4.1	120	4	3.3	2	-24	-2.7	4.49
4.1	124	0	0.0	1	-22	-1.8	3.06
4.1	88	0	0.0	1	-27	-1.2	2.07
4.1	90	9	10.0	2	-26	-0.8	1.4

	4.1	64	8	12.5	2	-22	-2.5	4.18
	4.1	480	24	5.0	2	-28	0.7	0
	4.1	64	0	0.0	1	-24	-1.8	3.06
	4.1	340	0	0.0	1	-28	-1.2	2.07
	4.1	410	0	0.0	1	-26	-0.8	1.4
	4.1	68	0	0.0	1	-25	-2.5	4.18
	4.1	92	0	0.0	1	-22	0.7	0
	4.1	120	0	0.0	1	-22	-1.8	3.06
	4.1	124	80	64.5	2	-27	-1.2	2.07
	4.1	88	0	0.0	1	-27	-0.8	1.4
	4.1	90	0	0.0	1	-24	0.7	1.23
	4.1	64	0	0.0	1	-22	-2.7	4.49
	4.1	480	0	0.0	1	-27	-0.4	0.35
	4.1	64	0	0.0	1	-27	-0.4	0.35
	4.1	90	0	0.0	1	-22	-1.3	2.24
	4.1	140	0	0.0	1	-22	-1.3	2.24
	4.1	220	0	0.0	1	-22	-1.4	2.41
	4.1	60	0	0.0	1	-24	-0.4	0.71
	4.1	44	9	20.5	1	-22	-2.5	4.18
	4.1	78	24	30.8	2	-26	-1.2	2.07
	4.1	54	0	0.0	1	-27	-0.8	1.4
	4.1	120	0	0.0	1	-22	0.7	0
	4.1	140	0	0.0	1	-27	-2.7	4.49
	4.1	52	0	0.0	1	-22	-0.4	0.71
	4.1	54	0	0.0	1	-27	-0.4	0.71
	4.1	48	0	0.0	1	-27	-1.3	2.24
	4.1	68	9	13.2	2	-22	-1.3	2.24
	4.1	140	0	0.0	1	-22	-1.4	2.41
	4.1	160	6	0.0	2	-24	-0.4	0.71
	4.1	90	0	0.0	1	-33	-2.5	4.18
Broken Cliffs	4.2	45	0	0.0	1	-34	-4.4	7.02
Upper Morgan	4.2	34	0	0.0	1	-34	-4.4	7.02
	4.2	46	0	0.0	1	-36	-4	6.45
	4.2	54	0	0.0	1	-36	-4	6.45
	4.2	576	0	0.0	1	-31	-2.6	4.34
	4.2	500	440	88.0	2	-31	-2.5	4.18

	4.2	480	220	45.8	2	-31	-2.5	4.18
	4.2	20	0	0.0	1	-32	-12.5	16.43
	4.2	20	0	0.0	1	-32	-12.5	16.43
Broken Cliffs	4.6	10	0	0.0	1	-36	-9.2	13.07
Upper Morgan	4.6	21	0	0.0	1	-33	-9	12.85
	4.6	21	0	0.0	1	-34	-9.6	13.51
	4.6	12	0	0.0	1	-37	-8.4	12.16
	4.6	40	0	0.0	1	-33	-8.8	12.62
	4.6	12	0	0.0	1	-33	-8.4	12.16
	4.6	16	0	0.0	1	-37	-9	12.85
	4.6	20	0	0.0	1	-37	-9.2	13.07
	4.6	22	0	0.0	1	-36	-9	12.85
	4.6	40	0	0.0	1	-33	-9.2	13.07
	4.6	36	0	0.0	1	-37	-8.6	12.39
	4.6	12	0	0.0	1	-37	-8.8	12.62
	4.6	14	0	0.0	1	-37	-8.4	12.16
	4.6	16	0	0.0	1	-37	-9	12.85
	4.6	10	0	0.0	1	-33	-8.6	12.39
	4.6	10	0	0.0	1	-35	-9.2	13.06
	4.6	18	0	0.0	1	-36	-9.2	13.06
	4.6	22	0	0.0	1	-37	-9.2	13.06
	4.6	14	0	0.0	1	-33	-9.1	12.96
	4.6	16	0	0.0	1	-34	-9.2	13.06
	4.6	12	0	0.0	1	-33	-8.4	12.16
	4.6	60	12	20.0	2	-37	-10	13.94
	4.6	40	0	0.0	1	-36	-19.2	21.82
	4.6	24	0	0.0	1	-34	-8.4	12.16
	4.6	62	14	22.6	2	-38	-9.8	13.72
	4.6	40	0	0.0	1	-34	-10	13.94
	4.6	48	10	20.8	2	-38	-10	13.94
	4.6	21	0	0.0	1	-37	2.1	0
	4.6	18	0	0.0	1	-36	2.1	0
	4.6	60	8	13.3	2	-34	-9.2	13.06
	4.6	34	9	26.5	2	-33	-8.4	12.16
	4.6	96	0	0.0	1	-37	-2.2	3.71
	4.6	64	0	0.0	1	-37	-2.2	3.71

	4.6	48	9	18.8	2	-38	-2.2	3.71
	4.6	24	0	0.0	1	-36	-2.2	3.71
	4.6	12	0	0.0	1	-33	-2.2	3.71
	4.6	68	12	17.6	2	-38	-2.2	3.71
	4.6	24	0	0.0	1	-38	-2.2	3.71
	4.6	60	0	0.0	1	-34	-2.2	3.71
	4.6	48	0	0.0	1	-37	-2.2	3.71
	4.6	80	36	45.0	2	-36	-8.6	12.39
	4.6	100	0	0.0	1	-37	-8.6	12.39
	4.6	70	0	0.0	1	-36	-5.7	8.81
	4.6	68	0	0.0	1	-36	-4.7	7.45
	4.6	48	0	0.0	1	-37	-3.8	6.16
	4.6	70	12	17.1	2	-37	-8.6	12.28
	4.6	42	0	0.0	1	-36	-5.2	8.14
	4.6	64	0	0.0	1	-37	-4.8	7.59
	4.6	56	0	0.0	1	-37	-3.8	6.16
	4.6	22	0	0.0	1	-36	-4.8	7.59
	4.6	124	24	0.0	2	-37	-8.6	12.39
	4.6	180	0	0.0	1	-37	-5.6	8.68
	4.6	42	0	0.0	1	-37	-5.6	8.68
	4.6	54	0	0.0	1	-37	-5.6	8.68
	4.6	12	0	0.0	1	-37	-3.8	6.16
	4.6	46	0	0.0	1	-37	-4.7	7.45
	4.6	78	0	0.0	1	-36	-3.8	6.16
Broken Cliffs	4.16	160	1.9	1.2	3	-42	-17.5	20.6	3 clear 1 pinkish bubble
Upper Morgan	4.16	7	2.0	28.6	3	-44	-18	20.97	2 clear, 1 pinkish bubble crystal ? -175 to -95 in pinkish bubble
	4.16	22	3.0	13.6	3	-43	-21	23.05	2 clear 1 pinkish bubble
	4.16	35	4.5	12.9	2	-44	-8.1	11.81	1 bubble at -44 to -8.2 & crystal? btn -175 & -95 in pink bubble
	4.16	21	8.0	38.1	2				N/A
	4.16	15	5.0	33.3	2				N/A
	4.16	45	2.5	5.6	2				N/A
	4.16	22	0.0	0.0	1				N/A
	4.16	48	0.0	0.0	1				N/A
	4.16	35	10.0	28.6	2				pinkish bubble rim

	4.16	85	5.4	6.3	2				thick bubble
	4.16	15	3.0	20.0	2				N/A
Sunlands PS	5.2	14	0.5	3.6	2	-36	-15	18.63	bubble back -18
Upper Morgan	5.2	16	1.0	6.3	2	-37	-13	16.89	bubble back -18
	5.2	24	1.0	4.2	2	-32	-8.8	12.62	
	5.2	12	1.0	8.3	2	-32	-8.9	12.73	
	5.2	32	1.0	3.1	2	-37	-9.3	13.07	bubble goes at -70, back at -17.9
	5.2	12	0.5	4.2	2	-37	-9.2	13.06	bubble goes at -79, back at +5.5
	5.2	37	0.5	1.4	2	-36	-18.6	21.4	bubble goes at -76
	5.2	39	3.0	7.7	2	-34	-21.5	23.18	
	5.2	24	1.0	4.2	2	-36	-9	12.85	
	5.2	20	1.0	5.0	2	-34	-8.8	12.62	
	5.2	34	1.0	2.9	2	-38	-9	12.85	bubble goes at -70
	5.2	24	2.0	8.3	2	-40	-9	12.85	bubble goes at -72
	5.2	18	0.5	2.8	2	-39	-12	15.96	
	5.2	18	1.0	5.6	2	-38	-8.2	11.93	
	5.2	28	1.0	3.6	2	-38	-8.8	12.62	
	5.2	26	3.0	11.5	2	-38	-9	12.85	bubble goes at -72
	5.2	30	1.0	3.3	2	-36	-9.4	13.29	
Overland Corner	10.1	11	4.5	40.9	2	-33	-16.5	19.84	
Overland Corner Clay	10.1	42	0.0	0.0	1	-33	-8.5	12.28	
	10.1	45	0.0	0.0	1	-32	-9	12.85	
	10.1	34	0.0	0.0	1	-34	-9	12.85	
	10.1	30	0.0	0.0	1	-33	-9.1	12.96	
	10.1	44	0.0	0.0	1	-33	-8.4	12.16	
	10.1	24	0.0	0.0	1	-33	-8.6	12.39	
	10.1	30	0.0	0.0	1	-33.5	-8.7	12.51	
	10.1	12	0.0	0.0	1	-33.5	-8.7	12.51	
	10.1	85	3.5	4.1	2	-33	-8.6	12.39	
	10.1	42	0.0	0.0	1	-33	-8.8	12.62	
	10.1	45	25.0	55.6	2	-37	-22	23.18	clear bubble went at -86, didnÕt come back
	10.1	54	4.0	7.4	2	-36	-21	23.05	clear bubble went at -86, back at -16
	10.1	128	17.3	13.5	2	-37.5	-16	19.45	grey bubble went at -47, back at -18, -1.9, -18, -19, -18.8

10.1	120	14.0	11.7	2	-37	-13	16.89	grey bubble went at -47, back at -21,+1.8, then didnÕt return
10.1	88	9.0	10.2	2	-35	-18	20.97	
10.1	64	8.0	12.5	2	-36	-16	19.65	
10.1	80	12.0	15.0	2	-36	-18	20.97	
10.1	130	14.0	10.8	2	-33	-18	20.97	
10.1	22	3.4	15.5	2	-34	-8.6	12.39	smooth ice -16, bubble back at -1,-5.2,-18
10.1	120	7.0	5.8	3	-46	2.4	0	cracks? at -72, bigger at -46, 2
								yellow cubes recrystalized as 1 at +1.8, then 2 again
10.1	28	3.4	12.1	2	-32	-8.8	12.62	bubble appeared after first freeze
10.1	32	0	0.0	1	-32	-9.3	13.18	
10.1	24	3.5	14.6	2	-33.3	-7.4	10.98	bubble appeared after first freeze, gone at -47
10.1	25	4.0	16.0	2	-39	-15.3	18.88	ice distorted bubble
10.1	32	0.0	0.0	1	-39	-15.3	18.88	

11.3 APPENDICES
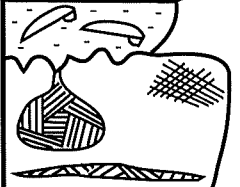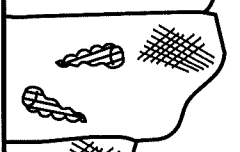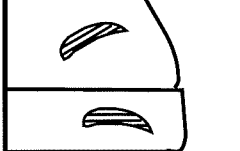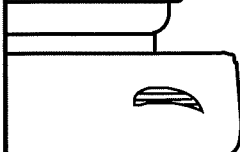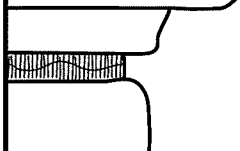
SECTIONS

Legend for stratigraphic sections

Lithology

Seed Gypsum

Laminated bed

Iron-staineed hardground

Sandstone

Well cemented hardground

Clay

Low angle cross beds

Scours

Limestone

Bedded Selenite

Meters

Clay	Marl	Calcarenite
Fine	Med.	Coarse Sand

Gypsum Nodules

Oyster

Selenite Nodule

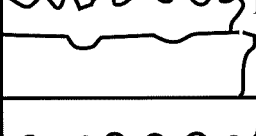Gypsum Filled Fossils

Gypsum Filled Cavities

Gypcrete
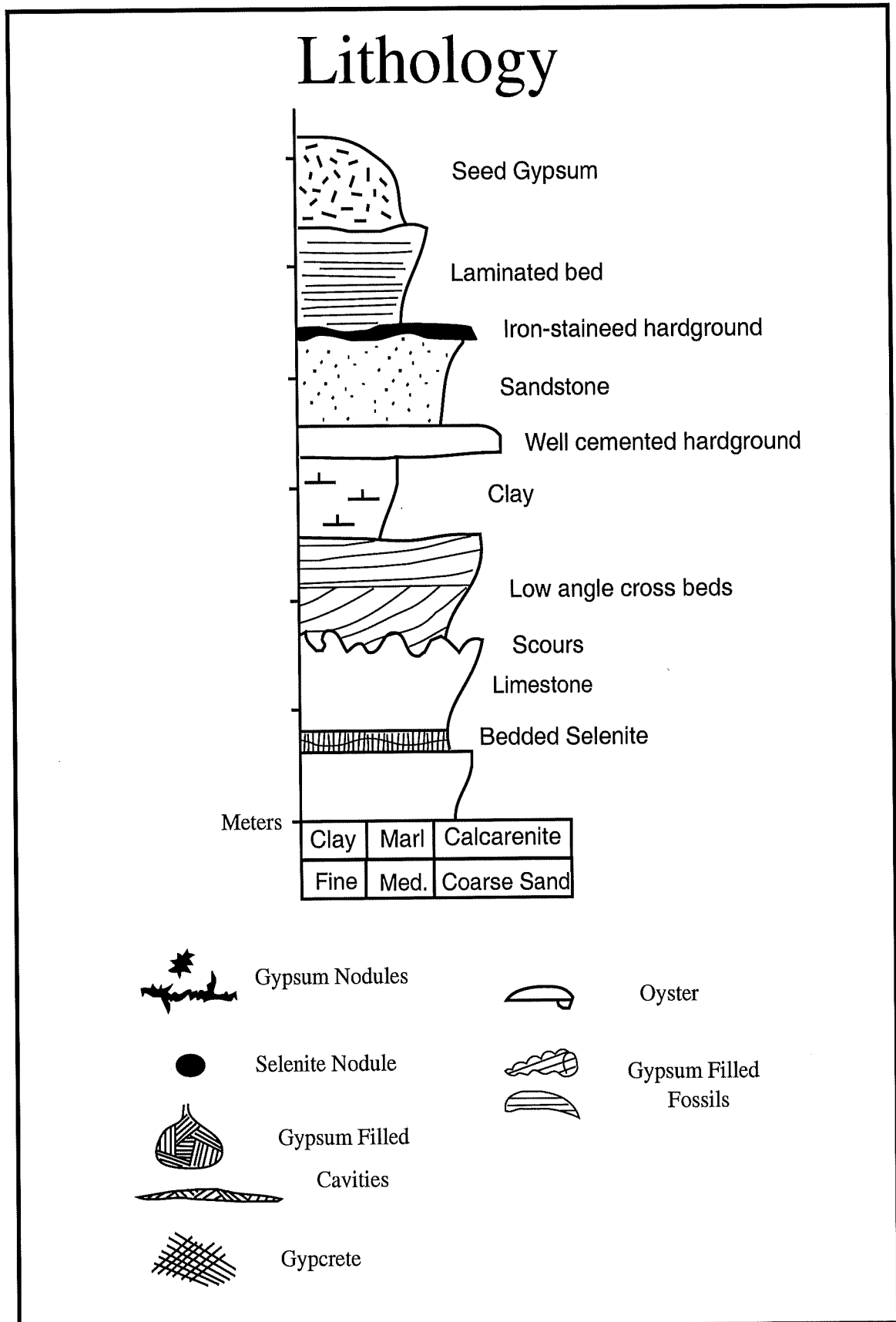
Broken Cliffs Section 2

34°06'46"S, 139°57'40"E

Age	Formation	Sample (A1129)	Lithology Clay	Marl	Calcarenite	m.

Pliocene — Norwest Bend Formation

Pale brown, ferruginised, coarse grained, calcareous sand containing abundant oyster shells — ~10

Medium grained, white, cross-bedded and laminated sandstone — ~9

Upper Miocene — Upper Morgan Limestone

Massive crystalline karst and void filling gypsum crust in calcarenite — ~8

Gypsum fossil pseudomorphs in pale yellow, massive, uniform marl — ~7 / ~6

Thin selenite layer — ~5

Gypsum fossil pseudomorphs in pale yellow, massive, uniform marl — ~4

Fine grained dolomitic calcarenite — ~2

4.12 Thick selenite layer in green clay — ~1
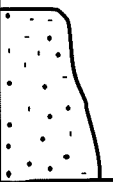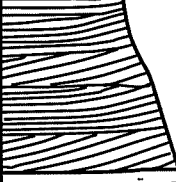
Broken Cliffs Section 1

34°07'03"S, 139°57'44"E

Age	Formation	Sample (A1129)	Lithology			m.
			Clay	Marl	Calcarenite	

Age column:
Pliocene
Upper Miocene (U p p e r, M i o c e n e)

Formation column:
Norwest Bend Formation
Upper Morgan Limestone

Lithology descriptions (top to bottom):

Pale brown, coarse grained, calcareous sand containing abundant oyster shells

Medium grained, laminated sandstone

Massive crystalline karst and void filling gypsum crust in calcarenite

Gypsum fossil pseudomorphs in pale yellow, massive, uniform marl

Thin selenite layer

Gypsum fossil pseudomorphs in pale yellow, massive, uniform marl

Fine grained dolomitic calcarenite

Thick selenite layer in green clay

Sample numbers: 4.6, 4.2, 4.1, 4.5, 4.11

Depth markers (m.): ~10, ~9, ~8, ~7, ~6, ~5, ~4, ~3, ~2, ~1

Sunlands Pumping Station
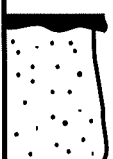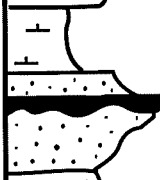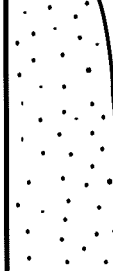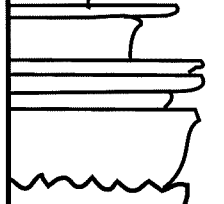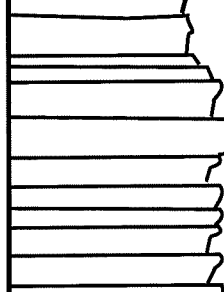
34°09'S, 139°55'E

Age	Formation	Sample (A1129)	Lithology			m.
			Clay	Marl	Calcarenite	

Lithology column descriptions (top to bottom):

- Pale brown to red, medium grained, soft, unstructured sand
- Brown, silicified hardground
- Cream coloured, medium to coarse grained, laminated sandstone
- Cream coloured, silicified medium to coarse grained sandstone
- Cream to pale brown, medium to coarse grained, laminated and cross-bedded sandstone
- Cream coloured, silicified medium to coarse grained sandstone
- Indurated hardground
- Yellow, coarse to fine grained, fossiliferous limestone
- Indurated hard ground in calcarenite
- Pale brown marl / calcarenite with small gypsum nodules and gutter casts
- Pale yellow, uniform, thin calcarenite beds
- Brown clay / marl

Age column: Quaternary; Pliocene; Upper Miocene

Formation column: Woorinen Formation; Loxton Parilla Sands; Patta Limestone; Upper Morgan Limestone

Sample (A1129): 5.2

Depth scale (m.): ~20, ~18, ~16, ~14, ~12, ~10, ~8, ~6, ~4, ~2

Overland Corner Section
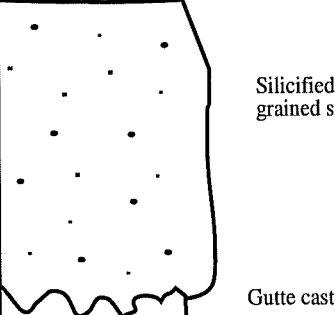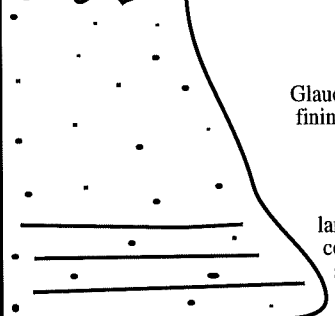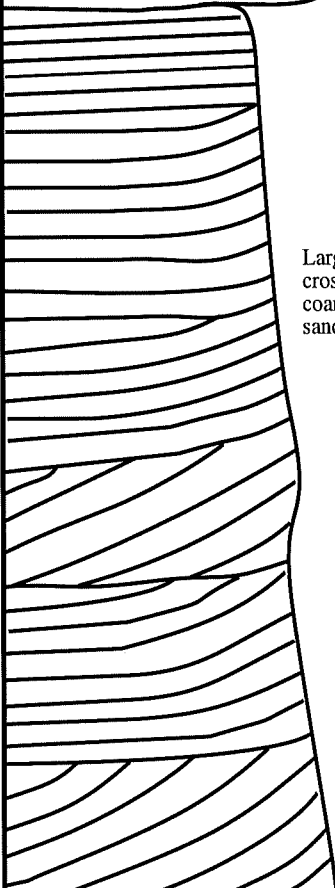
34°09'S, 140°20'E

Age	Formation	Sample (A1129)	Lithology	m.
			Clay / Marl / Calcarenite	
Quaternary	Woorinen Formation		Hard pink to brown silicified, hardground / Pale brown to red, medium grained, soft, unstructured sand	~30
Pliocene	Chowilla Sand		Green to brown clay / Hard pink to brown silicified, hardground / Pale brown, medium grained, soft, unstructured sand	~25 / ~20
	Blanchetown Clay		Green cracking clay with abundant gupsum nodules	
Miocene	Upper Morgan Limestone		Interbedded calcarenite and marl	~15
	Overland Corner Clay	10.1	Green cracking clay with abundant gypsum nodules	~10
	Lower Morgan Limestone		Pale yellow, massive, uniform marl / Pale yellow, uniform, thin calcarenite beds	~5

Modified after Lukasik and James (1998), and Kotsonis (1995).

Barmera Quarry

34°14'24"S, 140°26'E

Age	Formation	Sample (A1129)	Lithology				m.
			Clay	Fine	Medium	Coarse Sand	

Quaternary — Blanchetown Clay — Samples 12.3.1, 12.3

Green, cracking clay with prismatic gypsum nodules and rare celestite nodules ~10

Silicified, medium grained sandstone ~8

Gutte casts

Glauconitic sanstone, fining up sequence

laminated, pebbly, coarse glaconitic sandstone ~6

Large, low angle cross-bedding, coarse to medium sand ~4

~2

Pliocene — Loxton Parilla Sands

11.4 APPENDICES

THOMAS, B., BONE, Y. AND CLARKE, J., 1999. Fossil whale bones in the Middle Miocene Glenforslan Formation, Morgan. *Mines and Energy South Australia Journal, 15:32-33.*

Fossil whale bones in the Middle Miocene Glenforslan Formation, Morgan

Brett Thomas[1], Yvonne Bone[1] and Jonathon Clarke[2]

Introduction

Three whale vertebra and various bone fragments were discovered in early 1999 by Honours Geology student Brett Thomas in the town park at Morgan on the Murray River, South Australia (Fig. 1). The bones were found while a student group from the University of Adelaide was sampling a limestone embankment at the Morgan railway turntable. The turntable, formerly used on the wharf during the days of riverboat traffic, has been restored and forms part of the grassed public park adjacent to the river immediately below the main street of the town.

Watering of the surrounding lawns, and exposure for over 100 years, has caused the bones to become extremely weathered and crumbly, rendering exhumation difficult. Casts can be made however, and it is intended to display these in the Morgan Museum, which is conveniently located in the same park. An information board will probably be erected at the discovery site.

Fossil location fenced off in a limestone embankment at the Morgan railway turntable. (Photo 47083)

Regional geology

The Murray Basin, a shallow Tertiary, intracratonic basin covering ~300 000 km^2, comprises undeformed freshwater, marine, coastal and continental sediments of Paleocene to Quaternary age (O'Driscoll, 1960; Ludbrook, 1961; Thornton, 1974; Brown and Stephenson, 1991; Rogers *et al.*, 1995; Lukasik and James, 1998). Marine transgressions are restricted to the western part of the basin (Lawrence, 1973). The stratigraphy of the Oligo-Miocene section has recently

[1]*Department of Geology and Geophysics, University of Adelaide, 5000*

[2]*CRC LEME, Australian, National University, Canberra, 0200.*
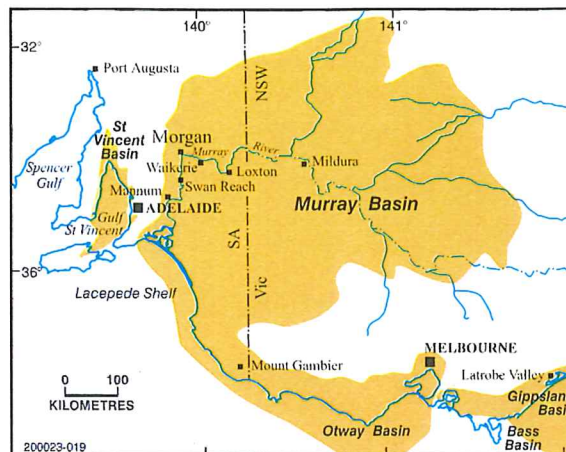

Fig. 1 Locality map (after Qianyu and McGowran, 1999).

been revised by Lukasik and James (1998; Fig. 2), and the entire time sequence elevated to the Murray Supergroup.

Three Middle Miocene (~16 Ma) Batesfordian and Lower Balcombian limestones together make up the Morgan Group. They constitute a 30 m thick succession of shallow, marine-platform, cool-water limestones of coarse-grained, bryozoan-dominated, skeletal debris, with varying proportions of calcareous clay, micrite and quartz sand. The Morgan Group is differentiated into the older Glenforslan Formation fossiliferous limestone, the middle marly Cadell Formation and the upper Bryant Creek Formation fossiliferous limestone.

Local geology

The small township of Morgan, on the western side of the Murray River where the river makes an almost right-angled bend towards the south (Fig. 1), is close to the north-westernmost extent of the Middle Miocene marine incursion. The Glenforslan Formation at Morgan is a mid-shelf facies bryozoan-rich limestone comprising large fragments of arborescent *Celleporaria* sp. (frequently mis-identified as *Celleporaria gambierensis*) within a matrix of fine to medium-grained fragments of articulated branching and delicate branching bryozoans (Bone and James, 1993) and foraminifera, and with lesser grains of fenestrate bryozoans, rare brachiopods, solitary ahermatypic corals, and localised patches of gastropods and echinoids. The limestone is locally but sparsely well cemented where the primary mineralogy of the components provided suitable cement (James and Bone, 1989).
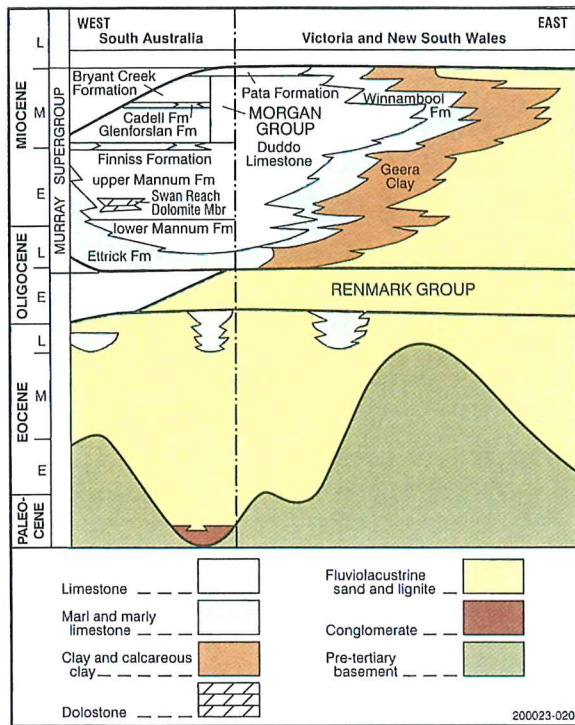
Fig. 2 *Stratigraphy of the Murray Supergroup (after Brown and Stephenson, 1991).*

Fossil whale bones at Morgan. (Photo 47084)

The whale bones occur within one of the uncemented, perhaps slightly deeper water layers. Three large vertebra, each 250–300 mm long, are partly exposed in a recessive, marly layer. The three bones and part of a fourth are still aligned, along with a number of smaller fragments, almost parallel to the embankment, suggesting that a large portion of the whale remains were removed during excavation for the turntable over 100 years ago. The bones are now light orange-brown in colour and still retain the spongy texture typical of whale bones, but the pore spaces are now filled with white phosphorite.

Whale bones in the Murray Basin

Most of the important developments of whale evolution were complete prior to the time of the Morgan whale in the Middle Miocene. Diversification of the ancestral Archaeocetes into the modern toothed and baleen whales occurred in the latest Eocene to Early Oligocene (Fordyce, 1992). The earliest representatives of modern families, such as Dephinidae (dolphins), Ziphiidae (beaked whales), Physeteridae (sperm whales), Balaenidae (right whales) and Balaenopteridae (rorquals), appear in the Late Oligocene to Middle Miocene. The Miocene was a period of high cetacean diversity at the family level (Fordyce, 1991), with almost all modern families represented as well as a number of extinct families, such as the Cetothere baleen whales and the squalodont toothed whales. Previous fossil whales from the Murray Basin are from the Pliocene. Miocene whales have been reported from the Otway Basin of Victoria (Fordyce, 1991). Detailed taxonomy of cetaceans is based mainly on the skull, and pos-cranial remains vary little after the Eocene (J. Daniels, University of Melbourne, pers. Comm., 1999). The Morgan whale is therefore likely to remain unclassified unless the skull can be found.
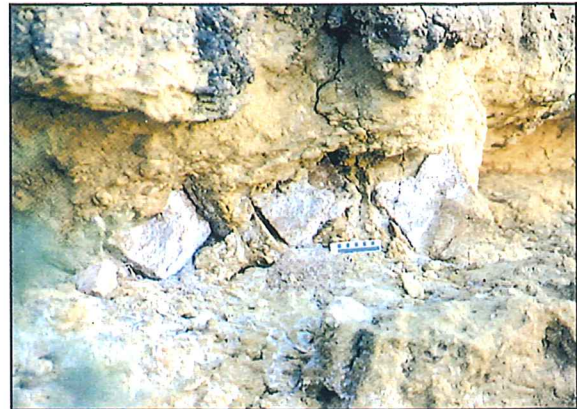
References

Bone, Y. and James, N.P., 1993. Bryozoa as sediment producers, Lacepede Shelf, southern Australia. *Sedimentary Geology,* 86:247-271.

Brown, C.M. and Stephenson, A.E., 1991. Geology of the Murray Basin, southeastern Australia. *Bureau of Mineral Resources, Geology and Geophysics, Australia. Bulletin,* 235.

Fordyce, R.E., 1991. The Australasian marine vertebrate record and its climatic and geographic implications. *In:* Vickers-Rich, P., Monaghan, J.M., Baird, R.F. and Rich, T.H. (Eds), *Vertebrate palaeontology of Australia.* Monash University Publications, Melbourne, pp.1166-1190.

Fordyce, R.E., 1992. Cetacean evolution and Eocene/Oligocene environments. *In:* Prothero, D.R. and Berggren, W.A. (Eds), *Eocene-Oligocene climatic and biotic evolution.* Princeton University Press, Princeton, New Jersey, pp.368-381.

James, N.P. and Bone, Y., 1989. Petrogenesis of Cenozoic temperate water calcarenites, South Australia: a model for meteoric/shallow burial diagenesis of shallow water calcite sediments. *Journal of Sedimentary Petrology,* 59:191-203.

Lawrence, C.R., 1973. Geology, hydrodynamics and hydrogeochemistry of the southern Murray Basin. *Victoria. Geological Survey. Memoirs,* 30(1).

Ludbrook, N.H., 1961. Stratigraphy of the Murray Basin in South Australia. *South Australia. Geological Survey. Bulletin, 36.*

Lukasik, J.J. and James, N.P., 1998. Lithostratigraphic revision and correlation of the Oligo-Miocene Murray Supergroup, western Murray Basin, South Australia. *Australian Journal of Earth Sciences,* 45:889-902.

O'Driscoll, E.P.D., 1960. The hydrology of the Murray Basin province in South Australia. *South Australia. Geological Survey. Bulletin,* 35(1).

Qianyu, L. and McGowran, B., 1999. Miocene foraminifera from the Finniss Clay and Cadell Marl, western Murray Basin: taxonomic and taphonomic contrasts and their environmental significance. *Alcheringa,* 23:133-152.

Rogers, P.A., Linday, J.M., Alley,N.F., Barnett, S.R., Lablack, K.L. And Kwitko, G., 1995. Murray Basin. *In:* Drexel, J.F. And Priess, W.V. (Eds), The geology of South Australia. Vol. 2, The Phanerozoic. *South Australia. Geological Survey. Bulletin,* 54:157-162.

Thornton, R.C.N., 1974. Hydrocarbon potential of Western Murray Basin and infrabasins. *South Australia. Geological Survey. Report of Investigations,* 41. ∎